INTERMETALLIC PHASE FORMATION AT Fe-Al FILM INTERFACES

GÜVENÇ TEMİZEL

SEPTEMBER 2006

INTERMETALLIC PHASE FORMATION AT Fe-Al FILM INTERFACES

A THESIS SUBMITTED TO
THE GRADUATE SCHOOL OF NATURAL AND APPLIED SCIENCES
OF
MIDDLE EAST TECHNICAL UNIVERSITY

BY

GÜVENÇ TEMİZEL

IN PARTIAL FULFILLMENT OF THE REQUIREMENTS
FOR
THE DEGREE OF MASTER OF SCIENCE
IN
METALLURGICAL AND MATERIALS ENGINEERING

SEPTEMBER 2006

Approval of the Graduate School of Natural and Applied Sciences

Prof. Dr. Canan Özgen
Director

I certify that this thesis satisfies all the requirements as a thesis for the degree of Master of Science

Prof. Dr. Tayfur Öztürk
Head of Department

This is to certify that we have read this thesis and that in our opinion it is fully adequate, in scope and quality, as a thesis for the degree of Master of Science.

Prof. Dr. Macit Özenbaş
Supervisor

Examining Committee Members

Prof. Dr.Çiğdem Erçelebi	(METU,PHYS)	_____
Prof. Dr. Macit Özenbaş	(METU,METE)	_____
Prof. Dr. Şakir Bor	(METU,METE)	_____
Prof. Dr. Ali Kalkanlı	(METU,METE)	_____
Prof. Dr. Cevdet Kaynak	(METU,METE)	_____

I hereby declare that all information in this document has been obtained and presented in accordance with academic rules and ethical conduct. I also declare that, as required by these rules and conduct, I have fully cited and referenced all material and results that are not original to this work.

Name, Last name : Güvenç, Temizel

Signature :

ABSTRACT

INTERMETALLIC PHASE FORMATION AT
Fe-Al FILM INTERFACES

Temizel, Güvenç

M.S., Department of Metallurgical and Materials Engineering

Supervisor: Prof. Dr. Macit Özenbaş

September 2006, 63 pages

This thesis presents the formation mechanism of intermetallics formed at Fe-Al film interfaces. Al thin films with different initial film thicknesses were coated on low carbon steel substrates by physical vapor deposition (PVD). By annealing the system at different temperatures and for different time intervals, several intermetallic phases were observed. X-Ray, SEM and EDS studies showed that intermetallic phases $FeAl_2$ and Fe_2Al_5 are most dominant phases which were observed and they formed sequentially on the contrary of intermetallics which formed synchronous in bulk materials.

Keywords: intermetallics, Fe-Al system, thin films.

ÖZ

Fe-Al FILM ARAYÜZEYLERİNDE METALLERARASI FAZLARIN OLUŞUMU

Temizel, Güvenç
Yüksek Lisans, Metalurji ve Malzeme Mühendisliği Bölümü
Tez Yöneicisi: Prof. Dr. Macit Özenbaş

Eylül 2006, 63 sayfa

Bu tez Fe-Al fim arayüzeylerinde oluşan metallerarası fazların oluşum mekanizmalarını sunmaktadır. Değişik ilk kalınlıklara sahip Al filmler düşük karbonlu çelik altlıklara fiziksel vakum kaplama (PVD) yöntemiyle kaplanmıştır. Sistemin değişik sıcaklıklarda ve değişik sürelerde bekletilmesi ile bazı metallerarası fazların oluşumu gözlenmiştir. X-Işınları Analizi, Tarama Elektron Mikroskobu ve EDS çalışmaları, en dominant faz olarak $FeAl_2$ ve Fe_2Al_5 metallerarası fazlarının gözlemlenmesini sağlamış, söz konusu fazların hacimsel malzemelerde görülen eşzamanlı oluşumun aksine sıralı olarak oluştuğunu göstermiştir.

Anahtar Kelimeler: metallerarası fazlar , Fe-Al sistemi, ince filmler.

To My Parents

ACKNOWLEDGMENTS

The author wishes to express his deepest gratitude to his supervisor Prof. Dr. Macit Özenbaş for his guidance, advice, criticism, encouragements and insight throughout the research.

TABLE OF CONTENTS

LIST OF TABLES

LIST OF FIGURES

CHAPTER 1

INTRODUCTION

In recent years, considerable effort has been devoted to the study of intermetallics. These unique class of metallic materials belong to intermediate compound family like carbides, oxides etc. and are formed during interdiffusion between two chemical species or two compounds.

Intermetallic compounds, especially bulk intermetallics, differ in a number of important ways from conventional metal alloys. Conventional alloys consist disordered solid solidification of one or more intermetallic elements. Alloys are mixtures of phases, where an intermetallic compound, on the other hand, has a definite atomic formula, with a fixed or narrow range of chemical composition. In conventional alloys, the atoms are linked with relatively weak metallic bonds. But, the bonds in intermetallics may be partly ionic or covalent and therefore stronger. Alternatively, the bonding may be entirely metallic, but the atoms of the individual elements take up preferred positions within the crystal lattice.

This ordering leads to an abrupt change in the properties of the material [1]. Some intermetallics have highly attractive elevated temperature strengths and these materials are not restricted to a single anecdotal structure but occur in a significant variety of ordered compounds. Their bonding is tighter than in the pure components of which they are formed, and they tend to have higher elastic stiffnesses and melting temperatures [2]. Most intermetallics exhibit brittle fracture and low ductility at ambient temperatures, poor fracture resistance and limited fabricability restrict their use as engineering materials in many cases [3].

They resemble the ceramics. But they have a metallic luster, conduct heat and electricity well [4 -5].

Among these ordered intermetallics, aluminides possess many attractive properties for structural use at elevated temperature in harsh environments.

These intermetallics have relatively low density, high melting point, good thermal conductivity, and superb high temperature strength. As a result these intermetallics are particularly suited for structural applications at elevated temperatures [6]. They also exhibit many peculiar properties that may find important applications in various fields in the form of thin films. In particular, it shows soft magnetic properties, such as low coercivity and high permeability, that makes it suitable for thin film type magnetic heads [7]. As use of thin films in electronics either as complete thin film circuits or more generally as interconnections and contacts in integrated circuits [8].Diffusion in thin, vacuum-deposited films is a phenomenon which has received significant attention [9].

To predict about occurrence and existence of these aluminides first a glance at the phase diagram of iron-aluminum system needed which reveals the existence of various equilibrium compounds. Moreover, growing thin films or multilayers, some metastable phases can arise due to interdiffusion and reactions occurring at temperatures much lower than in the bulk. This quite varied landscape stresses the importance of accurate microstructural characterization of the samples in connection with the growing processes and modalities [7] .

Reactive diffusion is a well defined approach at intermetallic formation which shows high dependency of both time and temperature. On the other hand in atomistic scale interfacial mixing behavior of the components gets importance.

The aim of this thesis was to study the intermetallic formation sequence at Al film -Fe system interfaces by the effects of annealing time, initial film thickness and temperature.

In chapter 2, intermetallic compound formation in thin film and in bulk samples is presented and also Fe-Al system intermetallic compound formation mechanisms and related literature survey is given.

Chapter 3 presents the experimental study and measurements which were made by using the X-ray diffraction (XRD), Scanning Electron Microscopy (SEM) and Energy Dispersive Spectroscopy (EDS) analysis. Experimental results were presented in Chapter 4 together with discussion. Finally, conclusions were given in Chapter 5.

CHAPTER 2

INTERMETALLIC COMPOUND FORMATION

2.1 Intermetallic Compound Formation In Thin-Film and In Bulk Samples

Considering a diffusion couple A/B between two metals or compounds. By an appropriate annealing, one expects to observe the formation of all the phases stable at this temperature according to the equilibrium diagram but at this stage, two different geometries must be considered; the infinite couple where the diffusion zone remains small as compared to the size of the specimen, and the semi-infinite samples and the thin samples, where at least one of the components has a small thickness. This is the case met with surface and thin film technologies as shown in Figure 2.1 [10].

For a unidirectional process all the intermediate phases would appear in the infinite couples as a series of parallel layers whose thickness will be increasing with time. On the contrary, in thin films or in semi-infinite samples, these phases appear sequentially (with time) and/or temperature, rather than simultaneously. The first compound grows until the exhaustion of one component, and a second compound will only appear later on [10]. That is the major difference between the two forms of the materials is that the intermetallic compounds form sequentially in thin films, while they tend to appear simultaneously in bulk samples.

Several factors influence the intermetallic compound formation, for example, the atomic diffusivities in various phases, concentration gradients, temperature, free-energy considerations, and impurities [9].

In studying thin film interdiffusion, it was quickly recognized that in a fine-grained thin film, the kinetic process is generally dominated by grain boundary diffusion, so that interdiffusion can occur faster than in bulk samples at lower temperatures [9].

The intermetallic formation and kinetics of the metal-metal interaction also strongly depend on the nature of the metal film (its thickness, grain size, purity, and defects), the substrate preparation, the interfacial oxides present, and the film deposition parameters (such as energy, temperature, and ambient pressure).

The most important factors controlling the nucleation of the first phase are as follows:

a) the cleanliness of the interface,
b) the diffusivity of metal atoms in each other,
c) the relative free energy of formation of various phases,
d) the temperature of interaction.

As far as only the diffusive part of the processes was analyzed, the full phenomenon involves two kinds of physicochemical processes:

1- The diffusion of components through each phase and
2- The transfer of component atoms at the interfaces between the phases.

Unfortunately for the latter there is no simple analogue to the Fick's Law with known (or at least measurable) diffusion coefficients, and one has to content himself with phenomenological laws derived from chemical kinetics to roughly describe the interface transfer processes as a chemical reaction.

It is usual to refer to these two kinds of processes as diffusion controlled and interface controlled. The interfaces play a key role for at least three reasons; the phase nucleation, the atomic transfer, the creation and/or annihilation of point defects.

For diffusion of an atom, two conditions must be met: (a) there must be an empty adjacent site, and (b) the atom must have sufficient energy to break bonds with its neighbor atoms and then cause some lattice distortion during the displacement. In most cases; $t^{1/2}$ dependence of the phase growth, parabolic growth, has been found, indicating a diffusion-limited growthIn some cases a linear dependence on time was found, suggesting an interface rate-controlled interaction. The growth rate of intermetallic compounds follows that equation;

$$t_h = D_0 e^{[-E/KT]}(t)^{1/2} \qquad (2.1)$$

where t_h is the intermetallic layer thickness,D_0 is a constant, E is the activation energy, k is the Boltzmann constant, T is the temperature, t is the time [11].

The single compound growth in thin films is a general phenomenon which has been studied by using X-Ray Diffraction, Rutherford Backscattering Spectroscopy, and Transmission Electron Microscopy, with a thickness detection limit around 200 A° for the first two techniques and better than 50 A° for the last one. In this situation, many phases of the thickness below the limits of detection may exist but were undetected in the film. To prove the absence of multiple phases in a diffusion couple requires a technique with a spatial resolution on the atomistic scale.

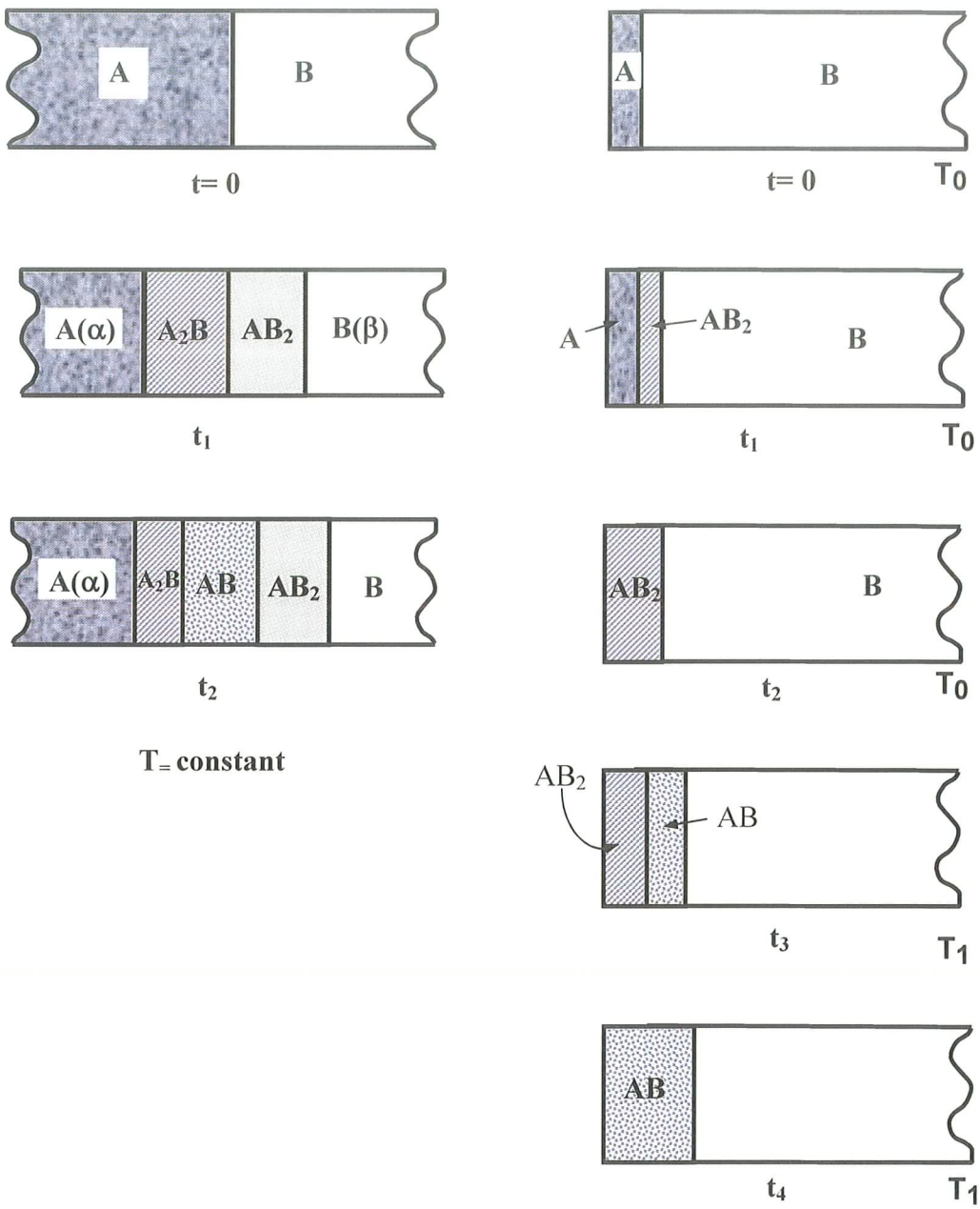

Figure 2.1 Schematic diagram illustrating the growth of two compound layers at the interface between two elements [10] .

Apart from the technological significance, there are particular advantages associated with the examination of diffusion in thin films, since it is possible to use experimental methods which can detect diffusion over extremely short distances as compared with bulk diffusion techniques, which generally involve sectioning in some manner. Bulk diffusion methods generally involve migration over distances of the order of microns whereas in thin films, diffusion over distances below 100 A° can readily be detected and measured. This means that the time of a diffusion anneal is correspondingly affected since diffusion frequently follows a parabolic law $x^2 \propto t$, and because of this, diffusion can often be examined at lower temperatures than are practicable with bulk diffusion couples, without involving unduly long annealing periods. At the same time, due attention must be paid to the possibility of excess vacancy concentrations in freshly deposited films and the possibility of grain-boundary diffusion which is likely to become relatively more pronounced at low temperatures.

Some investigators arrived at a conclusion that the thickness of each of the two layers, as well as their total thickness, should parabolically increase with time. In general, this is far from being the case. The thickness-time relationship in the case of two compound layers is very complex and only some portion of the curve is close to a parabola. Moreover, sometimes one of the layers only occurs after a considerable period of time while the other grows from the very beginning of the experiment [12].

2.2 Intermetallic Compound Formation In Fe-Al System

Multilayer structures based on the intermetallic phases of the Fe-Al system, obtained by solid state reactions, play an important technological role due to their applications as heat and corrosion resistant coatings for bulk

materials, metallization layers in microelectronic devices and magnetic recording head materials. In general, they exhibit soft magnetic properties and good mechanical quality even though their ductility at room temperature is very low [13].

The system Fe-Al has a complex equilibrium phase diagram revealing the existence of various equlibrium compounds and also exhibits a large variety of metastable non-equilibrium phases, (Figure 2.2).The system is characterized with an iron based solid solution and six non-stoichiomteric intermetallic compounds of Fe_3Al, FeAl, $FeAl_2$, Fe_2Al_3, Fe_2Al_5, $FeAl_3$. Table 2.1 indicates crytal structure and stability range for this phase diagram [14] .

There are two reasons for this behaviour. First, Fe and Al have a large difference in atomic radii as shown in Figure 2.3.Second, Fe exists in the flexible bcc lattice, whereas Al forms the dense packed fcc lattice. As a result up to 20 at. % of Al can be solved in Fe in thermodynamic equilibrium but only 0.04 at. % Fe in Al. Consequently, the Fe-rich side of the phase diagram shows only two phases (Fe_3Al and FeAl) with a simple structure and a large range of existence. On the Al-rich side of the phase diagram one finds several phases with a very complex structure and a narrow range of existence (for example $FeAl_2$, Fe_2Al_5, $FeAl_3$).

If Fe and Al are mixed by a non-equilibrium process such as mechanical alloying or ion-beam mixing the system has not sufficient time to form complicated phases, so metastable phases with a simple structure will be formed. The simplest structure is an oversaturated solid solution of Al in Fe and vice versa. Because of its flexibility, the bcc lattice of Fe can solve up to 70 at. % Al in the non-equilibrium case. For the inflexible FCC lattice a maximum of 7 at. % Fe has been reported [16]. In between these ranges (70-93 at. % Al) an amorphous structure is formed.

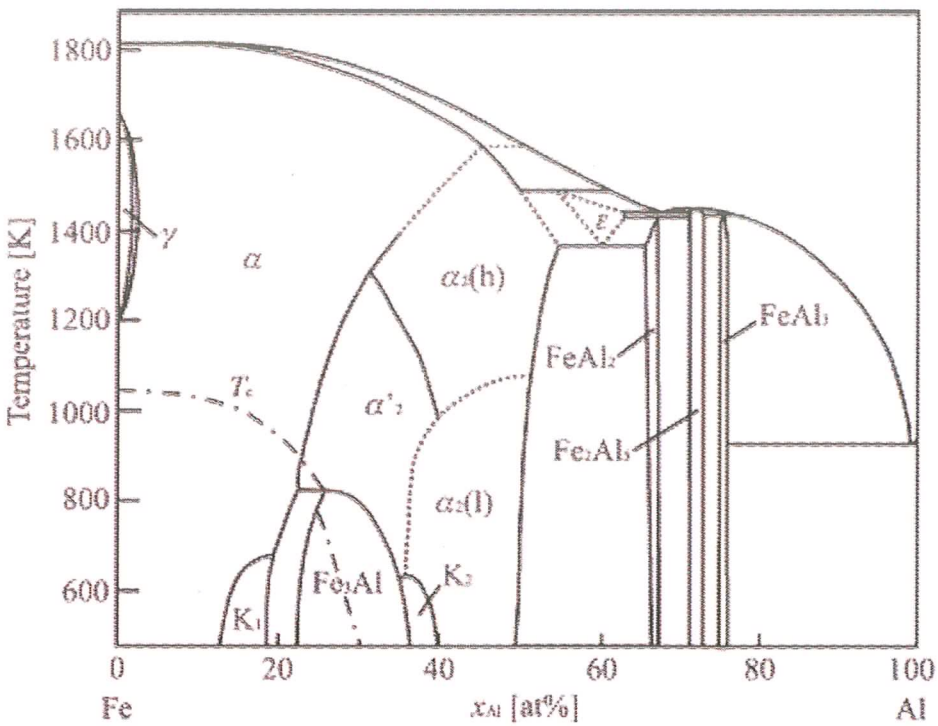

Figure 2.2 Fe-Al equilibrium phase diagram [14].

This non-equilibrium behavior is independent of the method that was used for mixing. The reported maximum amount of Al that can be solved in the bcc lattice differs from 50 at. % to 78 at. % without a correlation to the method [17.

It was shown that due to thermodynamic mixing a several-nm-thick transition region is formed between adjacent Fe and Al layers. The Fe-rich side of the transition layer is an oversaturated bcc solid solution, whereas the Al-rich side is an amorphous layer with an average composition of about $Fe_{20}Al_{80}$ [17].

Table 2.1 Crystal structure and stability range of the phases formed in Fe-Al binary system at room temperature [15] .These structures are presented in Appendix A.

Phases	Crystal Structure	Stability Range (at. %)
Fe solid solution	BCC	0-45
γ-Fe	FCC	0-1,3
FeAl	Ordered BCC (B2)	23-55
Fe_3Al	Ordered FCC (DO3)	23-34
Fe_2Al_3	Cubic (complex)	58-65
$FeAl_2$	Triclinic	66-66,9
Fe_2Al_5	Orthorhombic	70-73
$FeAl_3$	Monoclinic	74,5-76,5
Al solid solution	FCC	99,99-100

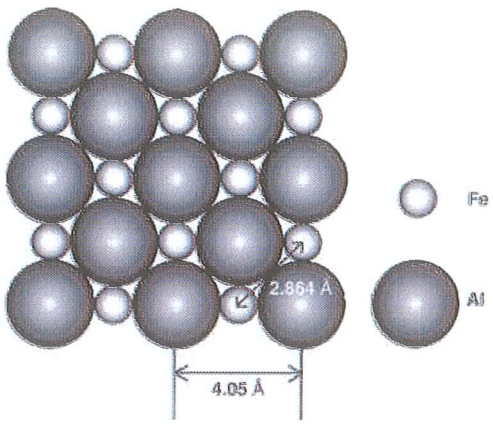

Figure 2.3 The schematic diagram of fcc-Al (001) surface with hollow sites occupied by bcc-Fe atoms [18].

Computer simulation based on a molecular dynamics approach is known to be a very effective way to investigate quantitatively on an atomistic scale the behavior of materials composed of thin films. Deposition behaviors of Fe adatoms on Al (001) substrates and Al adatoms on Fe (001) substrates were quantitatively investigated by molecular dynamics simulation to elucidate the interface characteristics and mixing phenomena [18].

The radial distribution function (RDF) peak of the intermixing region (i.e. the surface region of the Al substrate at the early stage of deposition) revealed that an FeAl intermetallic compound of FeAl structure was formed at the interface between Fe and Al.

The intermixing between the deposited Fe atoms and the Al substrate atoms could be clearly seen at the interface (Figure 2.4.a). On the other hand, a sharply distinct interface between Al and Fe was observed in the case of deposition of Al adatoms on Fe substrate at the same deposition conditions (Figure 2.4.b).

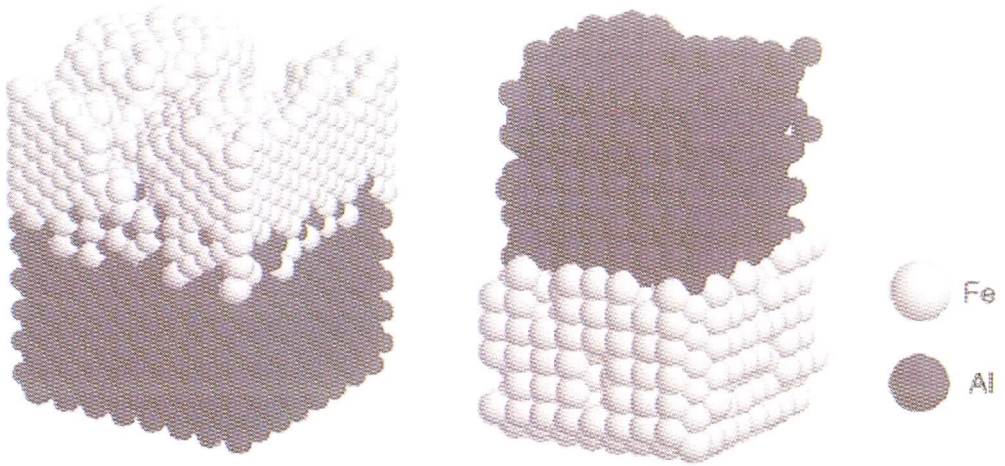

a) b)

Figure 2.4 a. Morphology of Fe/Al bilayer after the deposition of Fe atoms on Al substrate and b. Al atoms on Fe substrate [18].

The discrepancy of the morphology found at the interface region was reported to be due to the difference of the energy barrier between the penetration of Fe adatoms into the Al substrate and the reverse case [18].

Another aspect of the interfacial mixing behavior of the Fe/Al thin film system can be quantitatively analyzed by consideration of the local acceleration effect. Local acceleration is the sudden increment of kinetic energy of incident atoms in the vicinity of the substrate. The magnitude of local acceleration is known to be independent of the degree of the initial kinetic energy but dependent on the substrate orientation [19].

It can be concluded that the interfacial mixing was rather insensitive to the change of the initial kinetic energy of adatoms but largely dependent on the substrate temperature. The observation is consistent with empirical expectations,

i.e. interfacial mixing resulting from the diffusion of constituent atoms is strongly dependent on the temperature. The dissimilar mixing behavior at the interface between Fe/Al and other systems could be explained by the difference of cohesive energy, lattice matching, and the magnitude of local acceleration. It can be inferred that the interfacial mixing of the Fe/Al system was rather insensitive to the change in the initial kinetic energy of adatoms but largely dependent on the substrate temperature and orientation [18].

Another and important analysis on the iron-aluminum solid state diffusion couple was done by the aids of reactive diffusion approach [20].

Intermetallic layer at the interface grows as a result of annealing treatment and was observed experimentally the growth rate of aluminide increases with increasing temperature as shown in Table 2.2.

Table 2.2 Aluminide layer thickness at various annealing conditions [20].

Thickness	Time			
Temperature	1/6 h	½ h	1 h	1.5 h
500°C	7.03 μm	11.68 μm	16.13 μm	18.34 μm
550°C	11.5 μm	17.88 μm	24.35 μm	29.85 μm
600°C	15.57 μm	22.5 μm	32.9 μm	40.34 μm

On the other hand analysis of X-ray diffraction patterns clearly identified the phase to be Fe_2Al_5. In fact in the phase diagram of an Fe-Al system, there are several iron aluminide intermetallic compounds, such as Fe_3Al, FeAl, $FeAl_2$, Fe_2Al_5 and Fe_4Al_{13} [21].

First phase to form under this kind of solid-solid interaction can be predicted by EHF (effective heat of formation) theory proposed by Pretorius and coworkers [22]. The calculations were carried out for the solid-solid interaction in an iron-aluminum diffusion couple to figure out phase formation and found that the formation of Fe_4Al_{13} phase is kinetically favored. However on the other hand, thermodynamically, free energy of formation of Al-Fe compounds follows a reverse trend, i.e. $FeAl_2$ has lowest free energy of formation followed by Fe_2Al_5 and Fe_4Al_{13}[23]. Therefore it can be argued that despite thermodynamical drive, first phase to be form will be Fe_4Al_{13}. In the later stage, thermo-dynamic drive will overcome kinetic constraints and Fe_4Al_{13} and Fe phases will react with each other to form a phase with a composition between that of the interacting phases and closest to that of the eutectic composition i.e. Fe_2Al_5. That is the reason for not detecting Fe_4Al_{13} phase. Therefore, Fe_2Al_5 phase form due to direct reaction of iron and aluminum phases. This phase coincide with the Al-rich phase of the Fe-Al binary phase diagram. It can also be observed that the interface between Fe and Fe_2Al_5 appears irregular with peaks orientated towards the iron [20].

As the layer thickness bears a direct relation with growth kinetics, the average thickness of the aluminide layer has been used to understand and calculate the kinetic parameters involved in the diffusion couple studied. Growth of aluminide layer with time at 773 K is shown in the Fig. 2.5; it can be observed that growth rate decreases as layer thickness increases.

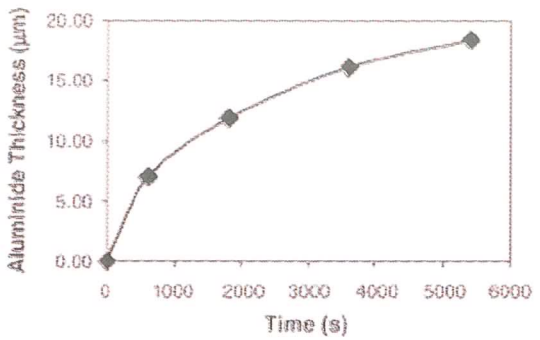

Figure 2.5 Growth of aluminide layer with time at 773K [20].

It seems to follow an inverse relationship with layer thickness in accordance with equation;

$$d\Delta x/dt=k/\Delta x \tag{2.2}$$

where Δx is the thickness of aluminide layer, k is the proportionality constant also known as parabolic rate constant.

Eq. (2.2) can be conveniently written in the form of Eq. (2.3).

$$\Delta x^2=2kt \tag{2.3}$$

In other words, thickness of aluminide layer is directly proportional to square root of time.

From the experimental data k is described as a function of T by the equation;

$$k=k_0\exp(-E_a/RT) \tag{2.4}$$

Here, k_0 is the pre-exponential factor, E_a is the activation enthalpy, and R is the universal gas constant.

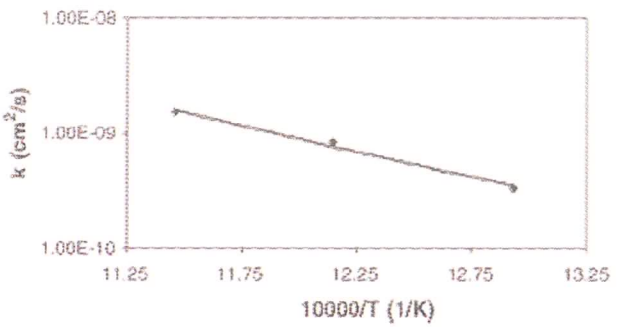

Figure 2.6 Parabolic rate constant for the growth of at Fe_2Al_5 773-873K [20].

The logarithms of k are plotted against the reciprocal of the annealing temperature as shown in Figure 2.6.As can be seen, the data points are located well on the corresponding straight line. The evaluation of Figure 2.6 provides k_0= 1.91 x 10^{-4} cm^2/s and E_a = 84.98 kJ/mol.

2.3 Fe-Al Thin Film Formation – Experimental Techniques and Findings

Aluminides can be formed by various ways by use of techniques of depositing films i.e. evaporation, sputtering, or chemical vapor deposition.

In the evaporation method a film is deposited by the condensation of the vapor on the substrate, which is maintained at a lower temperature than that of the vapor. All metals vaporize when heated to sufficiently high temperatures. Several methods, such as the resistive, induction, electron bombardment, or laser heating, can be used to attain these temperatures.

In sputter-deposition the target material is bombarded by the energetic ions to let loose some atoms. These atoms are condensed on a substrate to form a film. Sputtering processes are applicable to all materials-metals, alloys, semiconductors, and insulators. Cosputtering is simultaneous sputtering from two targets.

In chemical vapor deposition technique, the material, which forms a film on the substrate, is produced by a chemical reaction in the vapor phase or by a reaction that occurs on the substrate. Such depositions are limited only by the availability of the reactants that are in the gas phase or that will easily vaporize.

The deposited films must be annealed for research of the formation mechanism of intermetallics. Annealing conditions such as temperature, time, and ambient are determined by the type of the metal used. These conditions can be modified for each processing sequence.

Depending on the deposition process, different interface morphology can be achieved; interfaces deposited by thermal evaporation or sputtering are quite sharp, while those prepared by Pulsed Laser Deposition (PLD) at high pulse energy density show thick intermixed regions between adjacent layers [24 - 26].

Some of the recent studies and their findings are given below;

Fe-Al ML's (multilayers) submitted to thermal annealing between 375 to 775K were analyzed. The study revealed that the nucleation of the B2 phase occurred at 573 K and complete transformation of the ML in the defected B2 FeAl phase occurred at 673K annealing at higher temperatures or annealing more than 4 hours at 575 K only increased the structural order in the B2 phase [13].

It was proposed similar study like Mengucci preparing Fe-Al multilayers by two different types of laser deposition techniques; Direct Pulsed Laser Deposition (DPLD) and Crossed Beam Pulsed Laser Deposition (CBPLD). These are subjected to annealing between 50 and 950°C. Intermetallic phases formed in CBPLD and DPLD samples differ. Final compounds corresponded to known equlibrium phases. In CBPLD $FeAl_2$ and FeAl could be detected in the entire temperature range of full intermixing whereas $FeAl_2$ and $FeAl_3$ were found in the DPLD sample.Samples showed different reaction kinetics due to the differences in the interface composition of the as-deposited samples.A texture is developed for both types [27].

Fe-Al multilayers prepared by electron beam evaporation were studied. It was concluded that the diffusion of aluminum reasonably occurs along preferential paths in Fe, such as grain boundaries, establishing an Al concentration gradient. In Al-richer regions, Fe_2Al_5 forms and by decreasing the iron layer thickness, the Fe_2Al_5 contribution increases [7].

Powder liquid method was used for aluminization of steel substrates and submitted different thermal annealing cycles. The X-ray diffraction patterns of the aluminized substrates revealed different intemetallics formation with different types of slurry composition. Fe_3Al, FeAl, and Fe_2Al_5, $FeAl_2$ are detected. Specimens prepared with a fixed slurry of Al ratio applied and heated up to 973K or 1073K Fe_2Al_5, $FeAl_2$, FeAl, and alpha were identified [28].

CBPLD technique was used to form Al-Fe multilayers.Amorphous non-equlibrium state of the system was investigated.The results show that in a bulk system of Fe/Al alloys, amorphization takes place at Al concentrations above 75 at. % if Al and Fe are mixed by a non-equilibrium process such as ion-beam mixing. Just below this critical concentration the lattice is distorted to a non-cubic, Fe_2Al_5.-like structure. Above the critical concentration, the alloy is

amorphized by the formation of Al-Al pairs as Fe atoms do not incorporate the additionally introduced Al in their first two neighbouring shells.In thin films the high solubility of Al in bcc-Fe leads to the formation of a bcc solid solution.

This Fe-rich side of the transition layer is approximately twice as thick as expected from the kinetic energy of the particles. On the other side of the transition region the very low solubility of Fe in FCC-Al leads to the formation of an amorphous layer with a thickness of about 2 to 4 nm depending on the deposition sequence.The high contribution of the interfacial energy in a thin layer obviously stabilizes the amorphous phase and extends its range of existence to higher amounts of Fe. This confirms that the amorphous phase can be oversaturated with Fe, if it is within a thin-film system without cooling the substrate, a maximum Fe concentration in the amorphous Al-rich zone of about 30 at. % was found [17].

Table 2.3 summarizes the recent studies of Fe-Al system processed by different techniques and annealed at different temperature ranges. With an over look to these studies it can be concluded that intermetallics of Al rich side of Al-Fe phase diagram were observed. Moreover although stability range of some of these intermetallics such as $FeAl_3$ - Fe_2Al_5 - $FeAl_2$ are low and limited, they tend to be apparent regardless of processing technique. Nucleation and growth of phases in Fe-Al system depend on many factors. In reactive diffusion analysis diffusion parameters are assumed to be main factors for the formation of intermetallic phases. It is clearly stated and proved that thickness of a formed phase increase with temperature. On the other hand, growth rate of formation of one phase at constant temperature decreases as the film thickness increases. To analyze thin film formation with reactive diffusion approach, it can be concluded that formation of one phase is restricted with the other, i.e. exhaustion of one phase give rise to formation of other. Thermodynamically $FeAl_2$ intermetallic phase is most probable phase to be detected owing lowest free energy of

formation. Other phase of aluminum rich side of the Fe-Al phase diagram can be expected as well. Molecular dynamic simulation method is also used to analyze for the formation of intermetallic phases at Fe-Al system. In this case FeAl is found to be stable and its formation is related with cohesive energy, lattice matching and local acceleration effect. Behavior of intermixing is found to be dependent on substrate temperature.

Table 2.3 The results of recent studies of Fe-Al system.

Reference	Processing Method	Annealing Temperature	Intermetallics Detected
18	Computer Simulation	-	FeAl
20	Solid Sate Diffusion Couple	500°C	Fe_2Al_5
13	Electron Beam Evaporation	100°C -300°C	FeAl
27	Crossed-Beam Pulsed Laser Deposition	50°C -950°C	$FeAl_2$-FeAl
27	Direct Pulsed Laser Deposition	50°C -950°C	$FeAl_2$-$FeAl_3$
7	Electron Beam Evaporation	-	Fe_2Al_5
28	Powder Liquid Aluminization	-	Fe_3Al-FeAl-Fe_2Al_5- $FeAl_2$
28	Powder Liquid Aluminization	700°C -800°C	$FeAl_2$-FeAl

For the formation of Fe_2Al_5, need of Al rich regions such as grain boundaries are stated. Low iron layer thickness is also has the same effect for the formation of intermetallic phase Fe_2Al_5. Difficulty to predict thickness-time relationship in the case of two compound layers is always encountered. Complex situation prevents one model to work throughout. It is stated that one of the layers only occurs after a considerable period of time while the other grows from the very beginning of the experiment [12].

CHAPTER 3

EXPERIMENTAL PROCEDURE

The experimental work consisted of preparing steel substrates, vacuum coating of these steel substrates with evaporates, heat treatment of the films and examining the phases formed at the interface by using X-Ray Diffraction, Scanning Electron Microscopy and Energy Dispersive Spectroscopy studies.

Thin film samples of Al on low carbon steel (ASTM 1112 steel) substrates were prepared by resistive evaporation of pure Al thin wires. Resistive evaporation is probably the simplest vacuum deposition method. Other evaporation methods including primarily e-beam or a combination of e-beam and resistive evaporation can also be used. By a proper choice of the starting materials, the step including e-beam may be eliminated and thin film couples can be produced using a resistive evaporation.

3.1 Preparation of the Substrates

The Al films were grown on ASTM 1112 steel substrates about 5x5 mm^2 in size which were grinded on fine emery paper. To obtain a clean substrate surface, steel substrates were cleaned using a high-purity acetone and alcohol ultrasonic cleaner baths and immediately hot-air dried. After placing the steel substrates onto the substrate holder, the open surfaces of them were washed by pouring high-purity acetone and immediately dried in hot air. To remove any residual drops and dust particles, a handy blower was utilized just prior to placing the substrate holder in the vacuum chamber.

3.2 Coating of Al Films

For the deposition on the steel substrates, a vacuum deposition unit (Nanotech Thin Films Ltd., Model Microprep 300-S, Manchester, UK) was used. A tungsten filament, W, was used for vacuum evaporation of Al. The vacuum chamber was pumped out, the evaporant materials being previously placed. Deposition was not started before achieving a pressure of $1x10^{-4}$ Torr in order to produce sufficiently fast deposition rates and help the steel substrate surfaces to outgas to some extent without baking them. No substrate heating was applied other than the radiation heat from the source.

No control of any kind was applied to measure thickness or stoichiometry of the films. Placing appropriate amount of Al wire and evaporation-to-completion were the only tools for obtaining the desired thickness of the film. The distance between the steel substrate and the evaporation sources, after a few calibration attempts, was selected to be 2 or 4 cm, for which the starting materials were weighed to yield films of desired thickness upon complete evaporation of the materials in the W-basket.

3.3 Heat Treatment of the Films

A horizontal alumina tube furnace equipped with a programmable controller (ABB Kent Taylor - Commander 3000) was utilized in the post-deposition annealing of the films at 300°C, 500°C, 550°C and 650°C for the periods varying from 10 minutes to 8 hours in open alumina crucibles. The heating and cooling rates were set to +10°C/min and -1.5°C/min, respectively. The annealing process was carried out under flowing Ar. The Ar gas flow was maintained at a rate of 250 ml/min through the inner reaction tube having an

inner diameter of 3 cm. The gas was also bubbled in distilled water at the exit of the furnace for the purposes of creating the desired atmosphere inside the tube and observing the flow of the gas.

3.4 Characterization of Thin Film Samples

In this study, the structural properties of the samples were examined by using the X-ray diffraction (XRD), Scanning Electron Microscopy (SEM) and energy dispersive spectroscopy (EDS) analysis. The XRD studies were used to examine the structure of these films. SEM and EDS studies were conducted to investigate the microstructure and the surface morphology of the film samples

3.4.1 X-Ray Diffraction (XRD) Studies

After annealing procedure X-ray studies were carried out using a Philips Powder Diffractometer in the angle range between 30° and 90° with monochromatic Co-K_α radiation. Substrate peaks in the diffraction patterns of the samples were determined by using the previously taken patterns belonging to the steel substrate.

3.4.2 Scanning Electron Microscopy / Energy Dispersive Spectroscopy (SEM/EDS) Studies

The samples were further investigated by a Jeol JSM-6400 SEM equipped with an energy dispersive X-ray analyzer. During the SEM/EDS studies, both the film surface and its cross-section were examined. SEM samples were previously coated with a thin (25 nm) layer of gold-palladium alloy to prevent discharging of the specimen during examination. Final film thicknesses determined by SEM were about 2 μm to 14 μm.

CHAPTER 4

RESULTS AND DISCUSSION

In the experimental part Fe-Al system was studied. The purpose was to examine the formation mechanism of intermetallic phases which were formed at the interfaces of Fe-Al system. After deposition of the films, they were annealed at different temperatures and time intervals. X-ray diffractograms (XRD), Scanning Electron Microscopy (SEM) and Energy Dispersive Spectroscopy (EDS) studies were done in order to explain formation mechanism of the phases which were formed at the interface. The results of X-ray, SEM and EDS studies showed that intermetallics in the thin films formed sequentially on the contrary to the synchronous formation of intermetallics in bulk materials.

This chapter includes the detailed information of X-ray diffraction, SEM and EDS studies to explain this sequential formation of intermetallics in Fe-Al system.

4.1 X-Ray Diffraction (XRD) Analysis

After deposition of aluminum films having different initial thicknesses, they were annealed at different temperatures; 300^0C, 500^0C, 550^0C ,650^0C and for different annealing times; 10 min, 30 min, 1 h, 2 h, , 3 h, 4 h, 5 h and 8 h .

In Table 4.1, the intermetallic phases observed according to XRD and EDS analysis were listed within experimental conditions of initial thickness, annealing time and temperature. By a general approach to the table it could be concluded that intermetallics $FeAl_2$ and Fe_2Al_5 are two main detectable

aluminides. This information is consistent with the Table 2.3 (recent studies at Al-Fe system) where one or more of the intermetallics $FeAl_2$, Fe_2Al_5 and $FeAl_3$ were detected using different processing techniques having different annealing cycles. $FeAl_2$ is the most dominant phase that was observed almost at all experimental conditions. It is observed as only intermetallic phase mainly at higher initial film thickness values like 14 μm.

Additionally at lower initial film thickness or at higher annealing times intermetallic phase Fe_2Al_5 is also observed with intermetallic phase $FeAl_2$.

As can be seen in Table 2.2, at 300^0C there were three studies conducted. The intermetallic phases $FeAl_2$, FeAl and $FeAl_3$ were detected. These results are similar to the ones that are presented at Table 4.1. EDS analysis of Al films having an initial thickness of 2 μm annealed for ½ h, having an initial film thickness 3 μm annealed for 5 h and having an initial film thickness 8 μm annealed for 1h, showed the presence of Fe_2Al_3, $FeAl_2$ and $FeAl_3$, respectively. It can be also concluded that atomic % aluminum of the intermetallic phases formed increase with initial Al film thickness. As shown in Table 2.1 at % Al of Fe_2Al_3 is between 58-65 % .This intermetallic is observed at minimum initial film thickness (2 μm) whereas at % Al of $FeAl_2$ is 66-66.9 % a higher concentration when compared to Fe_2Al_3 and observed at a higher initial film thickness (3 μm) and finally at highest initial film thickness of 8 μm highest at % Al is observed for $FeAl_3$ which has at % Al between 74.5-76.5 %.

Although annealing process is carried under argon atmosphere, Fe_2O_3 phase is also observed on the films with an initial thickness of 2 μm, 3 μm and 8 μm starting at 4 hour of annealing. This behavior is attributed to the long annealing periods which cause some amount of oxidation in the samples.

Table 4.1 The intermetallic phases observed by annealing of Fe-Al films at different temperatures, times and initial thicknesses using XRD-EDS analysis.

		Initial Film Thickness			
Temperature	Time	2 μm	3 μm	8 μm	14 μm
300^0C	½ h	Fe_2Al_3			
	5 h		$FeAl_2$		
	1 h			$FeAl_3$	
500°C	1/6 h	$FeAl_2$ Fe_2Al_5			
	½ h	$FeAl_2$ Fe_2Al_5	$FeAl_2$	$FeAl_2$	
	1 h	$FeAl_2$ Fe_2Al_5	$FeAl_2$	$FeAl_2$	
	2 h		$FeAl_2$	$FeAl_2$	
	3 h		$FeAl_2$ Fe_2Al_5	$FeAl_2$ Fe_2Al_5	$FeAl_2$
	4 h	$FeAl_2$ Fe_2Al_5 Fe_2O_3	$FeAl_2$ Fe_2Al_5 Fe_2O_3	$FeAl_2$ Fe_2Al_5 Fe_2O_3	$FeAl_2$
	5 h		$FeAl_2$ Fe_2Al_5 Fe_2O_3	$FeAl_2$ Fe_2Al_5 Fe_2O_3	$FeAl_2$
	8 h				$FeAl_2$
550°C	4 h			Fe_2Al_5 Fe_3Al $FeAl_2$	
650°C	½ h		Fe_2Al_5 Fe_3Al $FeAl_2$		

In Figure 4.1, X-ray diffractograms are given for Al films having an initial thickness of 3 μm grown on steel substrates that were annealed for ½ h, 1 h, 2 h, 3 h, 4 h and 5 h at 500 ^{0}C as imposed on each other to visualize annealing time effect for the formation of intermetallics at constant initial thickness and annealing temperature. The intermetallic phase observed first is $FeAl_2$ as can be seen in the Figure 4.1 for ½ h, 1 h, and 2h With the increase in annealing time, Fe_2Al_5 was appeared after 3 hours.

Same results were observed for the films of an initial thickness of 8 μm. The results of X-ray diffractograms of Al films of an initial thicknesses of 8 μm grown on steel substrates that were annealed for ½ h, 1 h, 2 h, 3 h, 4 h and 5 h at 500 is shown at Figure 4.2 where intermetallic phase $FeAl_2$ is detected for all annealing time intervals of the study and on the other hand intermetallic phase Fe_2Al_5 is observed after 3 hours of annealing. From these graphs it could be concluded that at early stages of annealing intermetallic phase $FeAl_2$ owing relatively low concentration of aluminum is detected. At a longer period of annealing duration, Fe_2Al_5 is also observed owing a higher aluminum concentration. It is compared with the recent study of reactive diffusion of Fe-Al system at this temperature which is presented at section 2.2 [20]. These results appeared to be in the same line with each other. The formation of Fe_2Al_5 phase is observed in both studies. On the other hand the other studies $FeAl_2$ was stated as stable phase and encountered at a wide range of temperature interval of 50 ^{0}C to 950^{0}C [17]. Accordingly intermtallic phase $FeAl_2$ is expected at 500^{0}C which is proved in this study as well. Formation sequence of these phases can be related with two layer model of reactive diffusion where first a compound is formed and consequently a second favored through an appropriate time for diffusion supplied by the system. Generally, $FeAl_2$ which is the first phase observed showed an increase in its peak height until 3 hours of annealing time indicating that its amount is also increasing. However, with the start of formation of Fe_2Al_5 phase upon 3 hour annealing time, the peak height of $FeAl_2$ starts to decrease.

This behavior can be explained by the fact that longer annealing times cause the depletion of $FeAl_2$ phase in favor of the formation of the second phase Fe_2Al_5.

SEM micrograph of the 8 μm thick aluminum film grown on the steel substrate annealed for ½ h at 500 ^{0}C and X-ray diffractogram of the same film on which $FeAl_2$ detected is shown in Figure 4.3.a and 4.3.b, respectively. Similarly in Figure 4.4.a and 4.4.b, SEM micrograph of the 3 μm thick aluminum film grown on steel substrate annealed for 4 h at 500 ^{0}C and X-ray diffractogram of the same film showing the presence of $FeAl_2$ and Fe_2Al_5 intermetallic phases.

Annealing time and initial film thickness dependency of the intermetallics formed at the interfaces can be analyzed from these figures. As limited annealing time (½ h) was applied for the 8 μm thick aluminum film, only $FeAl_2$ intermetallic phase was observed, whereas the 3 μm thick aluminum film annealed for a longer period (4 h) revealed two different intermetallic phases ($FeAl_2$ and Fe_2Al_5) due to the enhancement of diffusion of Al into the steel substrate in this increased period of annealing time.

In Figure 4.5, X-ray diffractograms of Al films of an initial thickness of 3 μm grown on steel substrates that were annealed for ½ h at 650 ^{0}C and 4 h at 550 ^{0}C imposed on each other is shown. Intermetallics such as $FeAl_2$, Fe_2Al_5, and Fe_3Al were observed for both situations. High temperature of 650^{0}C which is very close to melting point of aluminum (660^{0}C) speeds up the diffusion process revealing the formation of several intermetallic phases of $FeAl_2$, Fe_2Al_5, and Fe_3Al. When compared with 650^{0}C, at relatively low annealing temperature of 550 ^{0}C again no difference achieved at the detected intermetallic phases which were $FeAl_2$, Fe_2Al_5, and Fe_3Al. This is due to longer annealing period (4 h) applied at this temperature, i.e., enhances diffusion of aluminum into steel substrate which is reported that when thin films of aluminum heat treated

between 400^0C and 660^0C leads to the irreversible growth of aggregates. At high temperatures (> 600^0C), the patterns grow very quickly (in a few minutes). At lower temperatures, the process is much slower [29]. On the other hand it was reported that sometimes one of the layers only occurs after a considerable period of time while the other grows from the very beginning of the experiment [12]. This behavior could be also a root reason for the formation of these phases at once.

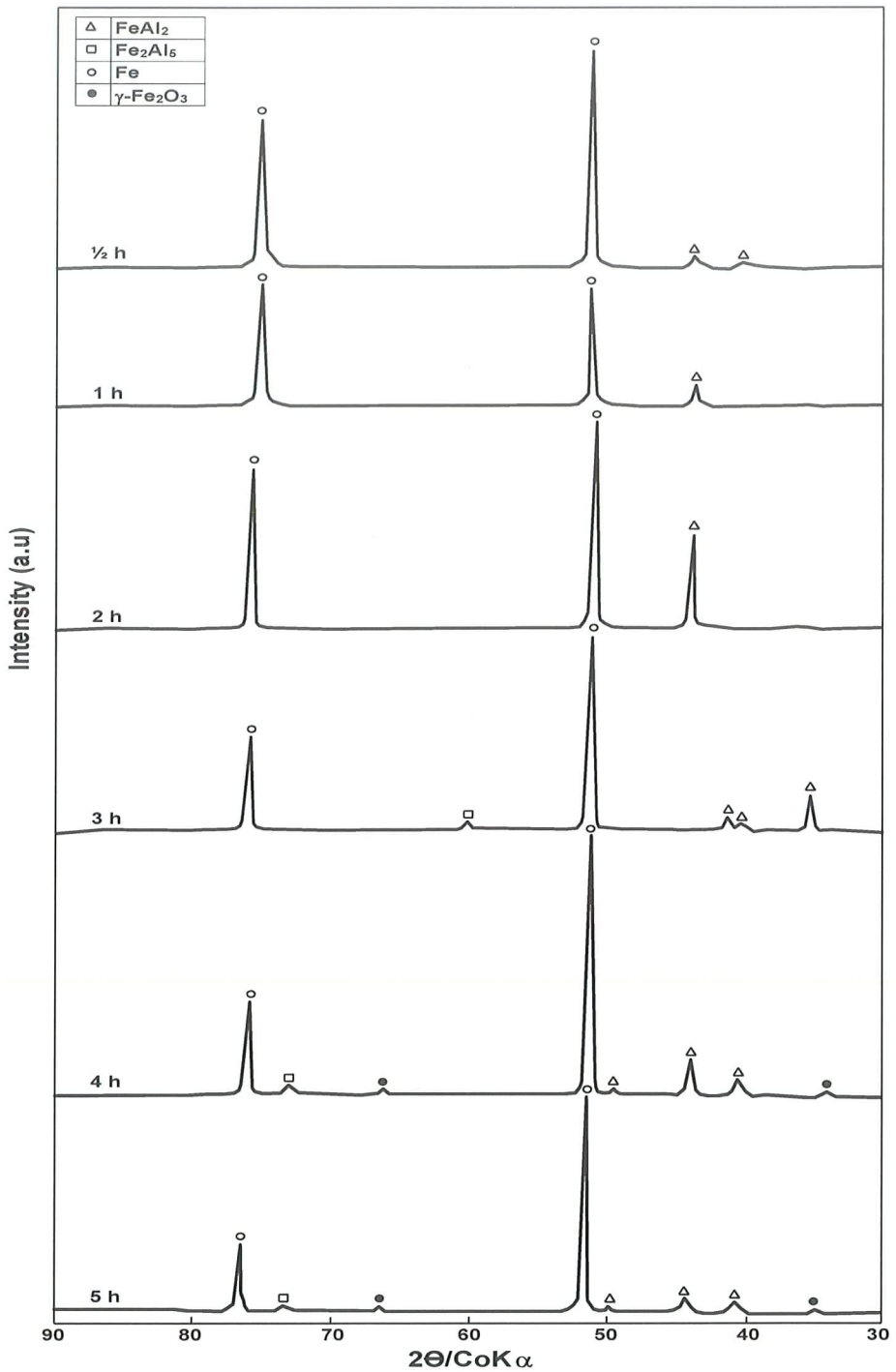

Figure 4.1 X-ray diffractograms of Al films of an initial thickness of 3 μm grown on steel substrate annealed for ½ h, 1 h, 2 h, 3 h, 4 h and 5 h at 500 ^{0}C.

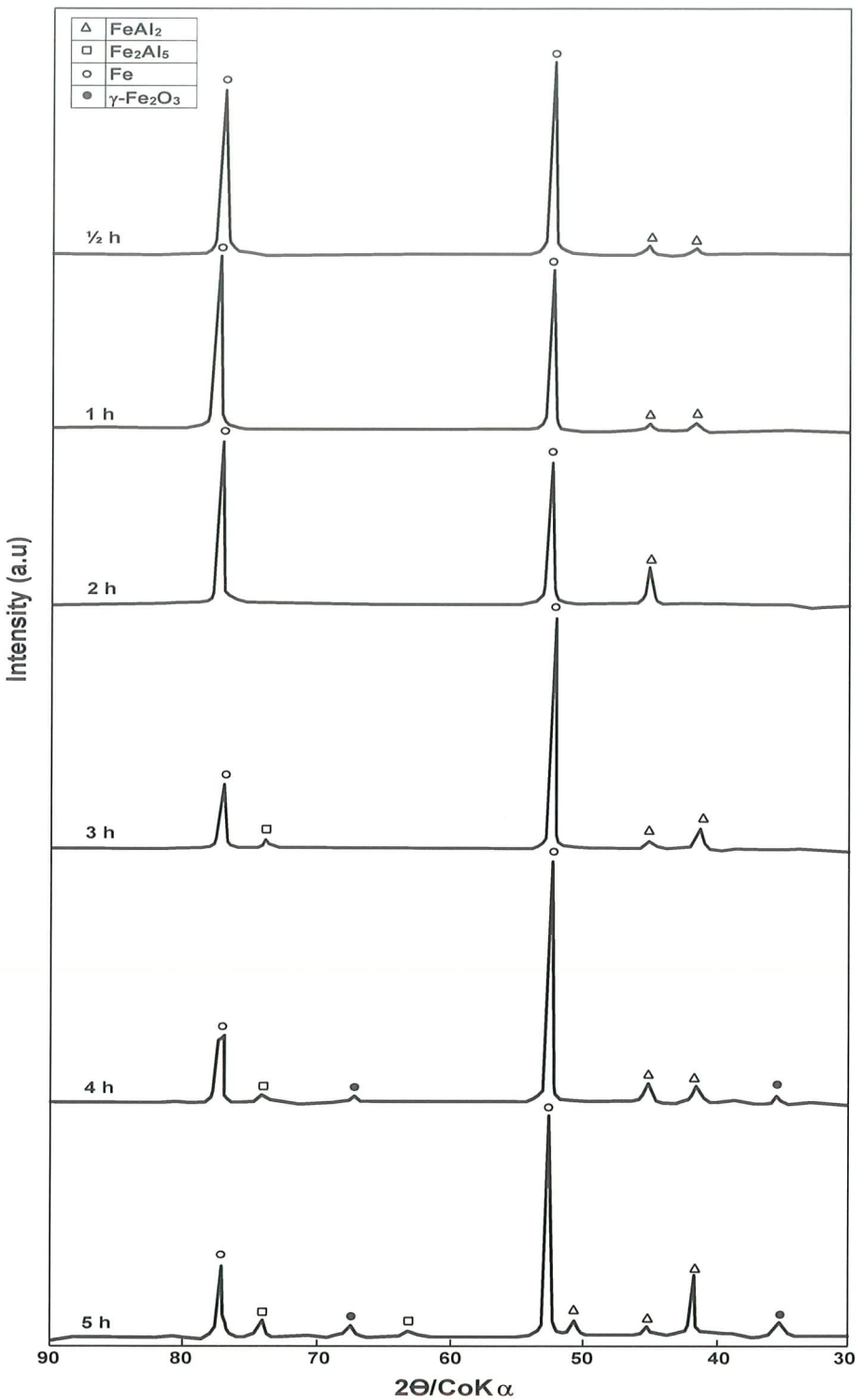

Figure 4.2 X-ray diffractograms of Al films of an initial thickness of 8 μm grown on steel substrate annealed for ½ h, 1 h, 2 h, 3 h, 4 h and 5 h at 500 ^{0}C.

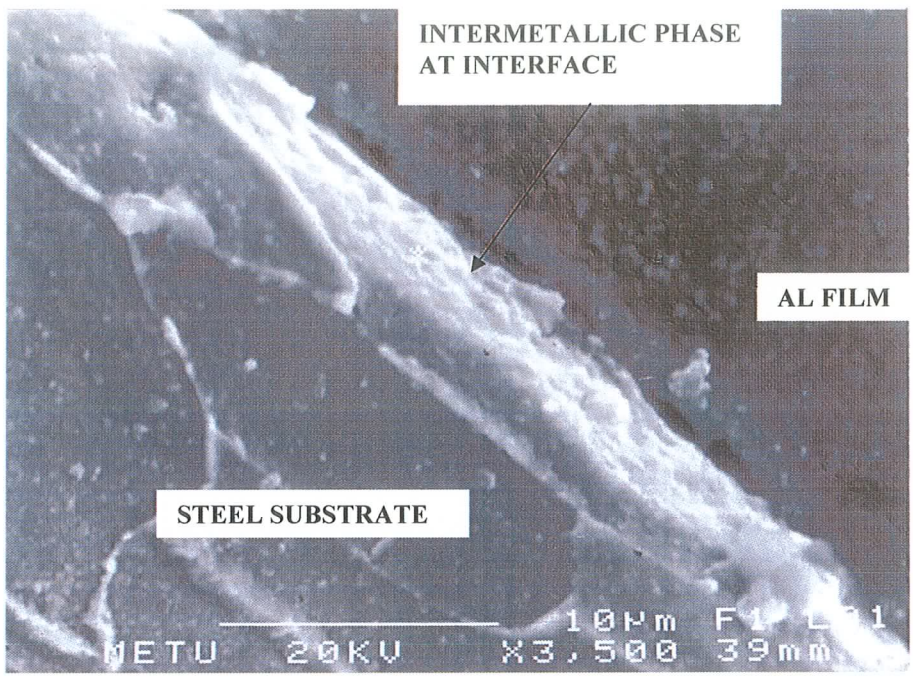

a)

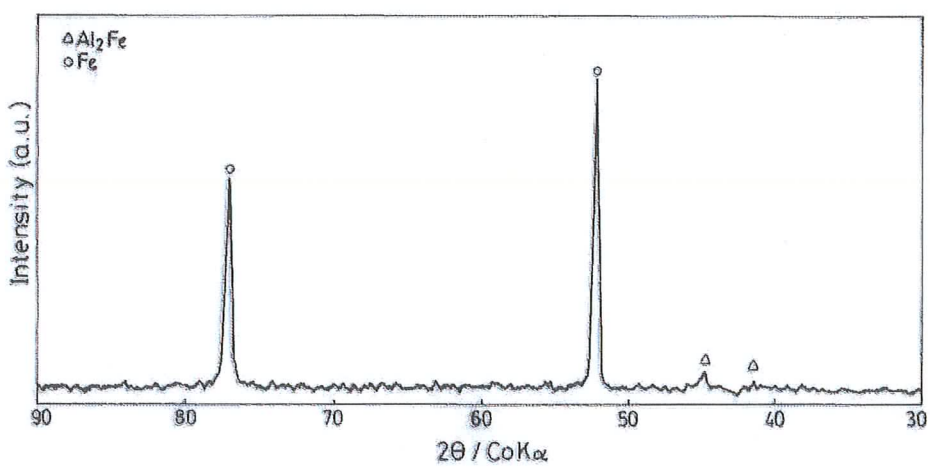

b)

Figure 4.3 a. SEM micrograph of 8 μm thick aluminum film grown on steel substrate annealed for ½ h at 500 ^{0}C **b.** X-ray diffractogram of the same film showing the presence of $FeAl_2$.

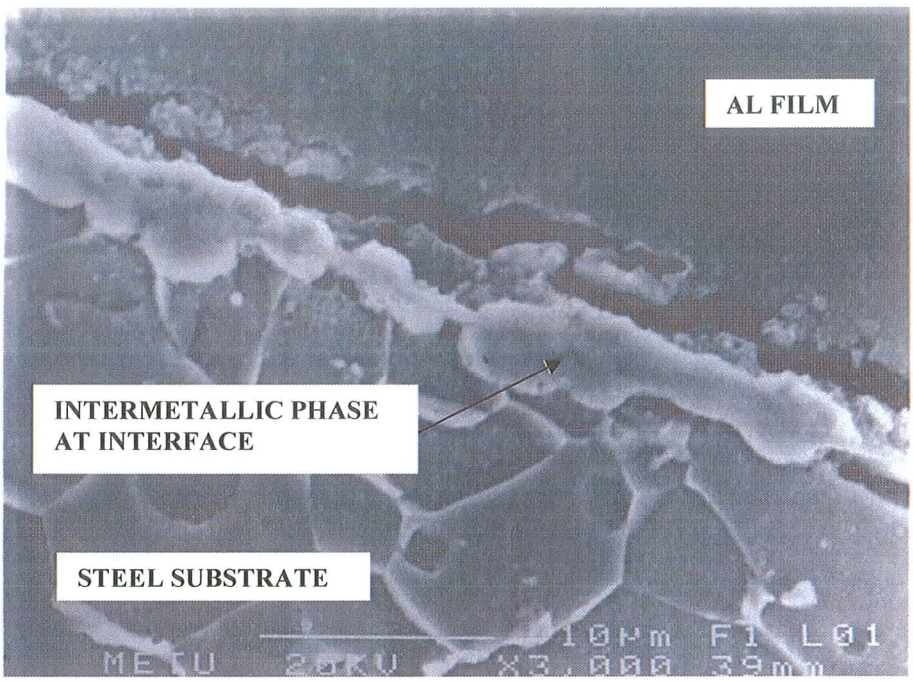

a)

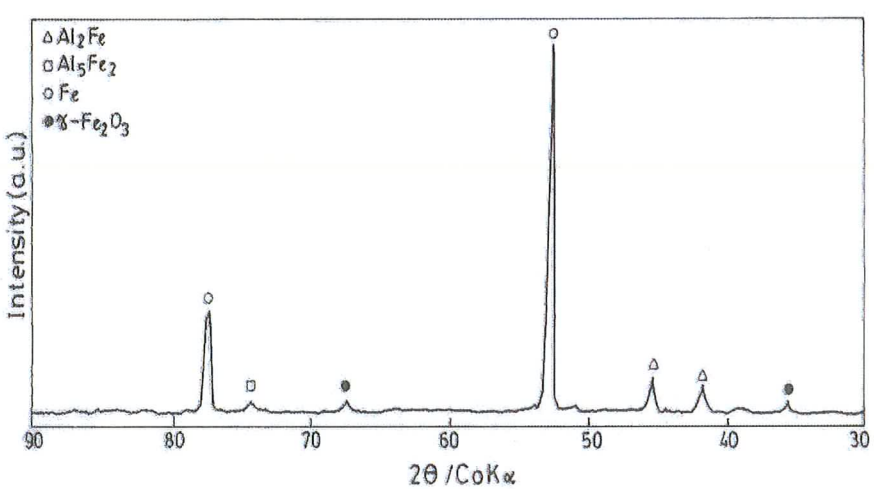

b)

Figure 4.4 a. SEM micrograph of 3 μm thick aluminum film grown on steel substrate annealed for 4 h at 500 ^{0}C, **b.** X-ray diffractogram of the same film showing the presence of $FeAl_2$ and Fe_2Al_5.

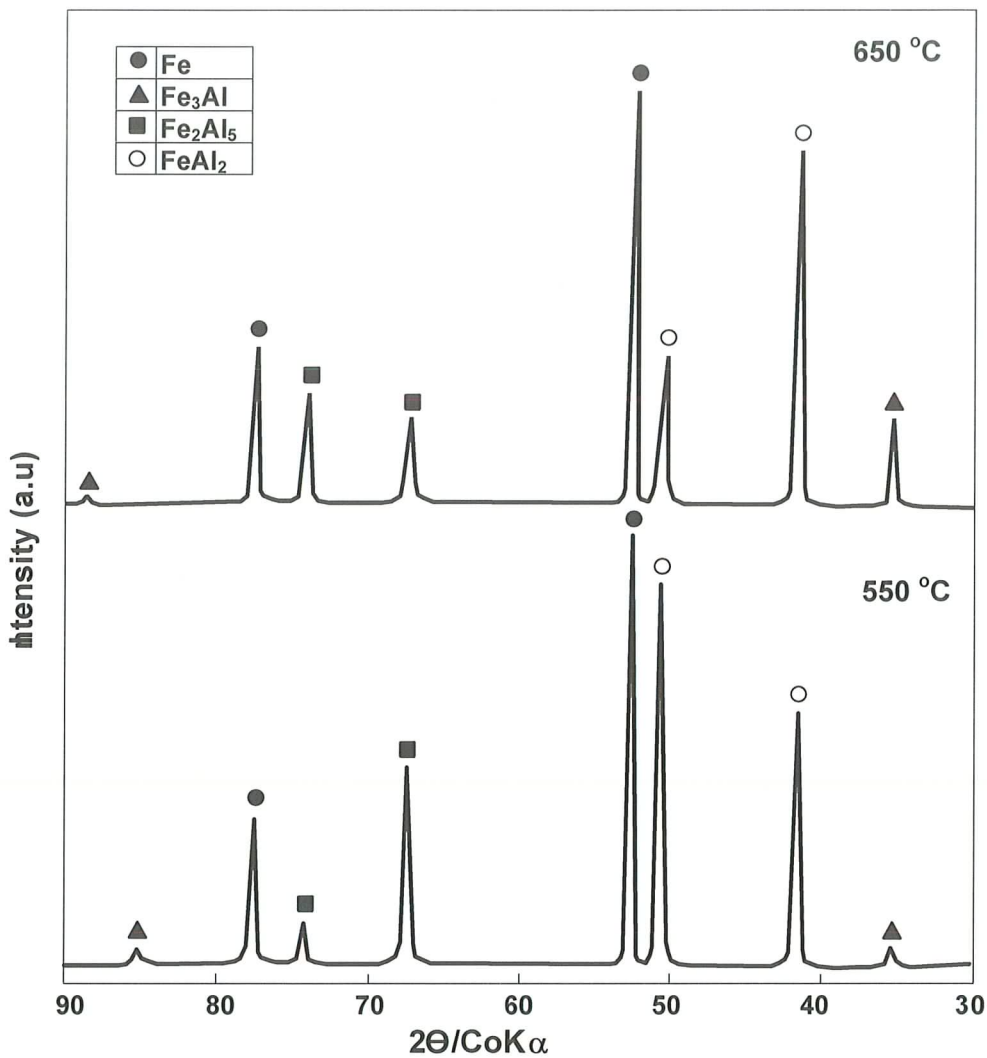

Figure 4.5 X-ray diffractograms of Al films of an initial thickness of 3 μm grown on steel substrate annealed for ½ h at 650^0C and 4 h at 550 ^{0}C.

4.2 Scanning Electron Microscopy (SEM) and Energy Dispersive Spectroscopy (EDS) Analysis

In this section selected SEM micrographs and EDS spectrums taken from cross sections of Fe-Al interfaces are presented.

In Figure 4.6, SEM micrograph of 2 μm thick aluminum film grown on steel substrate without annealing is shown. No crystalline phase is observed and because of coating method homogeneous but at the same time amorphous structure is obtained. It was taken as a reference micrograph for the interpretation of further SEM studies in which crystalline phases of aluminides were detected through XRD and EDS analysis.

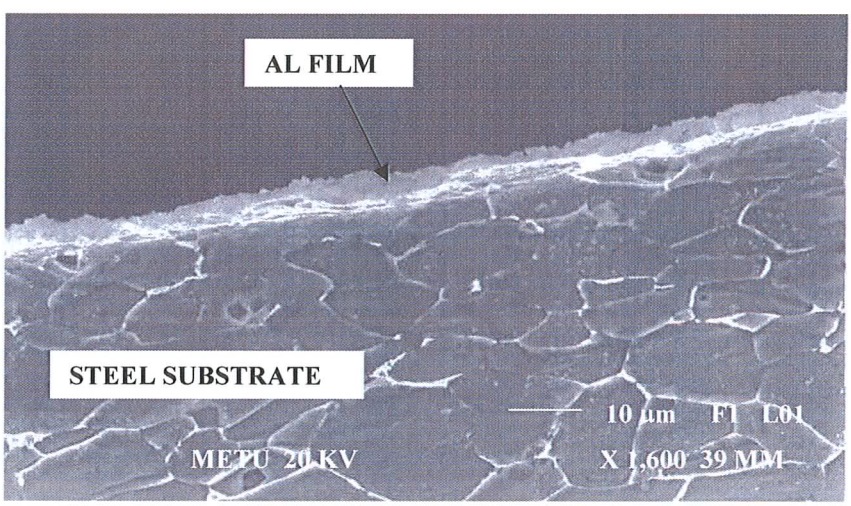

Figure 4.6 SEM micrograph of the 2 μm thick aluminum film grown on steel substrate without annealing

The results of EDS analysis of the intermetallic phases observed by annealing at different temperatures are given in Table 4.2. Atomic percentages are converted to probable respective intermetallic phases by the help of stability range determined at Table 2.1

These results support and strengthen the XRD analysis of the same specimens and in the same line with recent studies presented at section 2.3. $FeAl_2$, Fe_2Al_5, $FeAl_3$ are commonly encountered intermetallics. $FeAl_2$ is the most dominant phase that was observed. At mainly at higher initial film thickness values intermetallic phase $FeAl_2$ is observed whereas intermetallic phase Fe_2Al_5 is also observed with intermetallic phase $FeAl_2$ at relatively low initial film thickness like 2 μm.

In Figure 4.7.a and 4.7.b, SEM micrograph and EDS spectrum with general elemental distribution are shown for the cross-section of the aluminum film with an initial thickness of 2 μm grown on steel substrate annealed for ½ hour at 300^0C.Similarly same type of SEM micrographs and EDS general elemental distribution results are shown at the same temperature of 300^0C for a an initial thickness of 3 μm for 5 hours in Figure 4.8.a and 4.8.b, respectively. The last data of SEM micrograph and EDS analysis at 300^0C are shown in Figure 4.9.a and 4.9.b.The initial film thickness is 8 μm where annealing period is 1 hour. The intermetallic phases of Fe_2Al_3, $FeAl_2$ and $FeAl_3$ were observed at the above mentioned experimental situations, respectively. These results are consistent with the study of A.A. Levin, D.C. Meyer, P. Paufler, A. Gorbunov, A. Tselev, P. Gawlitza where $FeAl_2$, $FeAl_3$ and FeAl were detected at the same temperature at their experiments. As it mentioned at Section 4.1 at % of aluminum cocnetration of the intermetallic phases is increasing with increase at initial film thickness.

Table 4.2 The results of EDS analysis of the intermetallic phases observed by annealing at different temperatures – the numbers represents atomic percentages of the respective phases

Initial Film Thickness	Heat Treatment Temperature-time	Phases Observed
2 μm	300^0C-½ h	(Fe:38,61 Al:61,39)→Fe_2Al_3
2 μm	500^0C-½ h	(Fe: 27251 Al:72,75)→ Fe_2Al_5 (Fe: 33,96 Al:66,04)→ $FeAl_2$
2 μm	500^0C-4 h	(Fe: 29,87 Al:70,13)→ Fe_2Al_5
3 μm	300^0C-5 h	(Fe: 33,27 Al:66,73)→ $FeAl_2$
3 μm	500^0C-½ h	(Fe: 34,36 Al:65,64)→ $FeAl_2$
3 μm	500^0C-2 h	(Fe: 34,44 Al:65,56)→ $FeAl_2$
3 μm	650^0C-½ h	(Fe: 28,51 Al:71,49)→Fe_2Al_5 (Fe: 23,07 Al:76,98)→ $FeAl_3$
8 μm	300^0C-1 h	(Fe: 24,57 Al:75,43)→ $FeAl_3$
8 μm	500^0C-2 h	(Fe: 32,79 Al:67,21)→ $FeAl_2$
8 μm	500^0C-3 h	(Fe: 33,68 Al:66,32)→ $FeAl_2$
8 μm	500^0C-4 h	(Fe: 32,54 Al:67,46)→ $FeAl_2$
8 μm	500^0C-5 h	(Fe: 36,02 Al:63,98)→ $FeAl_2$
8 μm	550^0C-4 h	(Fe: 34,76 Al:65,24)→ $FeAl_2$
14 μm	500^0C-3 h	(Fe: 33,27 Al:66,73)→ $FeAl_2$
14 μm	500^0C-4 h	(Fe: 33,09 Al:66,91)→ $FeAl_2$

In Figure 4.10.a and 4.10.b, SEM micrograph and EDS spectrum with general elemental distribution are shown for the cross-section of the aluminum film with an initial thickness of 3 μm grown on steel substrate annealed for ½ hour at 500^0C. $FeAl_2$ intermetallic phase was observed. This result is also mentioned at Figure 4.1 with its XRD analysis. The experimental conditions of moderate initial film of 3 μm and low annealing time of ½ h revealed the formation of most dominant intermetallic phase $FeAl_2$ but as there is not enough driving force i.e. time, no other phase was detected.

Similarly same type of SEM micrograph and EDS general elemental distribution results are shown at the same temperature of 500^0C for an initial thickness of 8 μm for 3 hours in Figure 4.11.a and 4.11.b, respectively. In this case $FeAl_2$ phase at point 1 and Fe_2Al_5 phase at point 2 were observed. This figure could be interpreted with the Figure 4.3.a and 4.3.b, where SEM micrograph of the 8 μm thick aluminum film grown on the steel substrate annealed for ½ h at 500 ^{0}C and X-ray diffractogram of the same film on which detecte $FeAl_2$ intermetallic phase is shown. At the same experimental conditions of initial film thickness of 8 μm and annealing temperature of 500 ^{0}C only intermetallic phase $FeAl_2$ is observed at annealing period of ½ h where at longer period of annealing (3 h) both intermetallic phase $FeAl_2$ and intermetallic phase $FeAl_5$ was observed. These two figures are helpful to strengthen the propasal that is stated at Section 4.1 as longer annealing times cause the depletion of $FeAl_2$ phase in favor of the formation of the second phase Fe_2Al_5.

SEM micrograph and EDS analysis at 500^0C is shown in Figure 4.12.a and 4.12.b. The initial film thickness was 14 μm where annealing period was 3 hour. The intermetallic phase of $FeAl_2$ was observed. Same intermetallic compound was observed at the same initial thickness and temperature conditions when annealed for a longer time of 8 h as shown in Figure 4.13.a and 4.13.b. It could be concluded that for both experimental conditions (14 μm - 3 h - 500^0C

and 14 μm - 8 h - 500^{0}C) mentioned high initial film thickness contribution is high avoiding the formation of intermetallic phases other than the $FeAl_2$. Apparently it could also be concluded that with an initial film thickness of 14 μm intermetallic phase $FeAl_2$ is stable for a long period of annealing time at 500^{0}C. It is expected to be the same situation for lower temperatures as one of the important driving force factor of diffusion is lowered in this case.

In Figure 4.14, SEM micrograph and EDS analysis of Al film of an initial thickness of 3 μm grown on steel substrates that were annealed for 4 h at 550 ^{0}C is shown where presence of intermetallic phase $FeAl_2$ is observed. Similarly in Figure 4.15, same studies is shown for Al films of an initial thickness of 8 μm grown on steel substrates that were annealed for ½ h at 650 ^{0}C where presence of Fe_2Al_5 is observed. These figures strengthen the data of X-ray diffractograms of the same films shown at Figure 4.5, where $FeAl_2$ Fe_2Al_5 and Fe_3Al intermetallic phases observed.

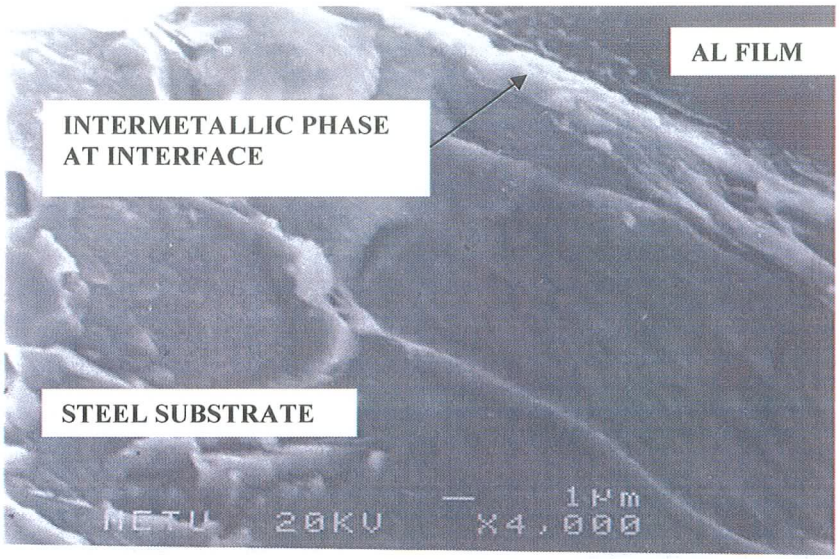

a)

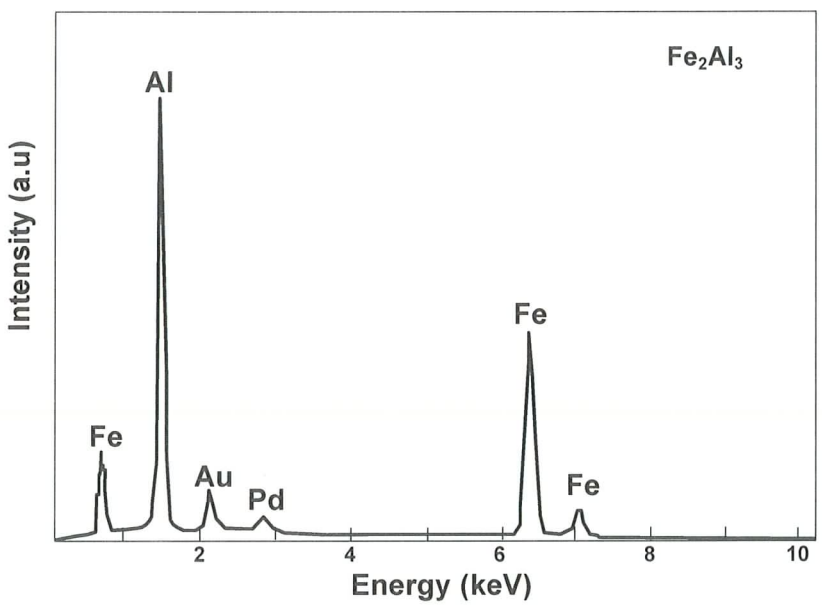

b)

Figure 4.7 a. SEM micrograph of the 2 μm thick aluminum film grown on steel substrate annealed for ½ h at 300^0C, **b.** EDS spectrum of point "1" showing the presence of Fe_2Al_3 at the interface.

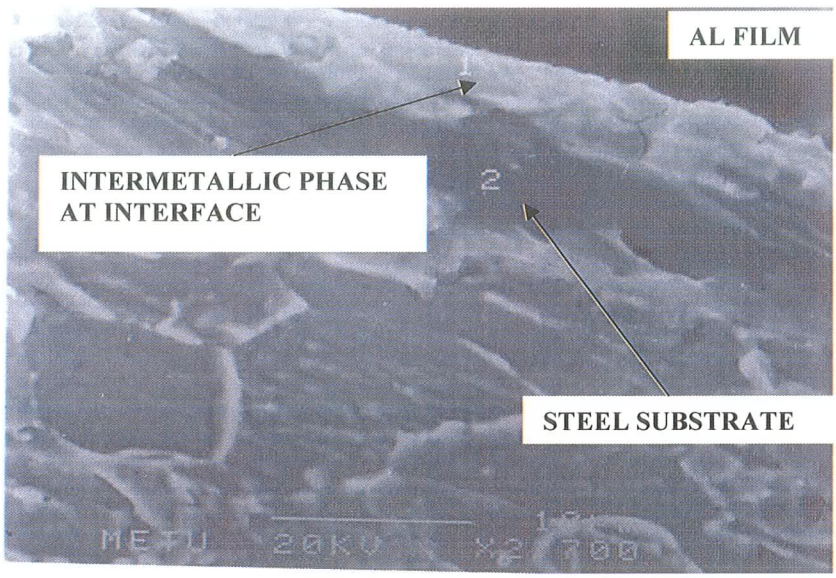

a)

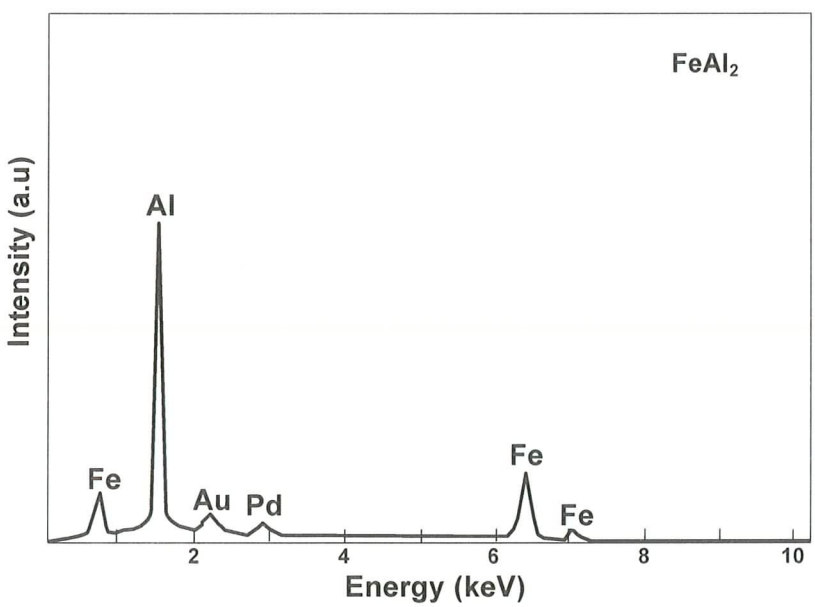

b)

Figure 4.8 a. SEM micrograph of the 3 μm thick aluminum film grown on steel substrate annealed for 5 h at 300^0C, **b.** EDS spectrum of the same film at point "1" showing the presence of $FeAl_2$ and point "2" is steel substrate.

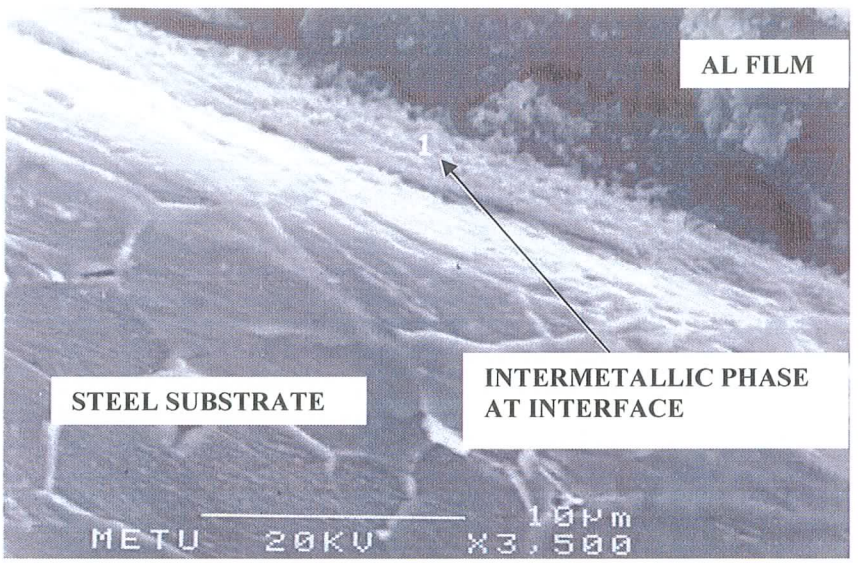

a)

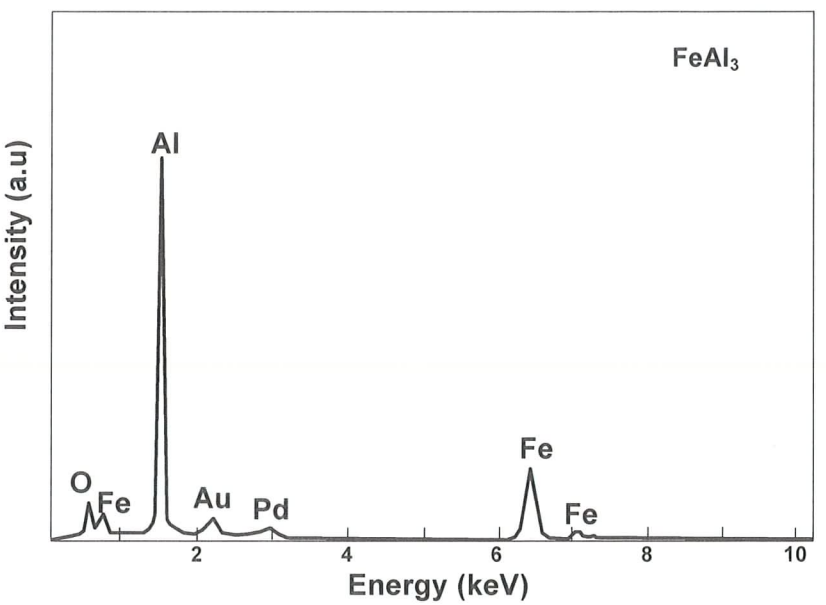

b)

Figure 4.9 a. SEM micrograph of the 8 μm thick aluminum film grown on steel substrate annealed for 1 h at 300^0C, **b.** EDS spectrum of the same film at point "1" showing the presence of $FeAl_3$.

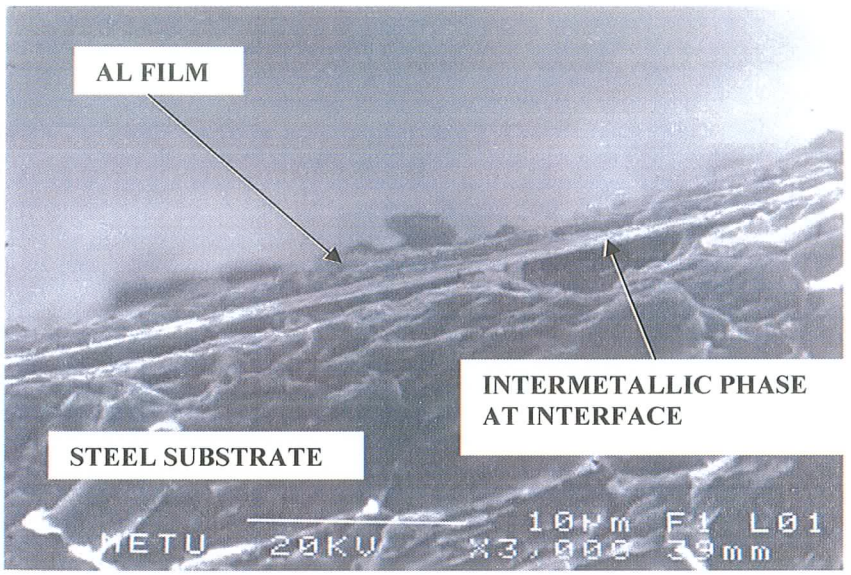

a)

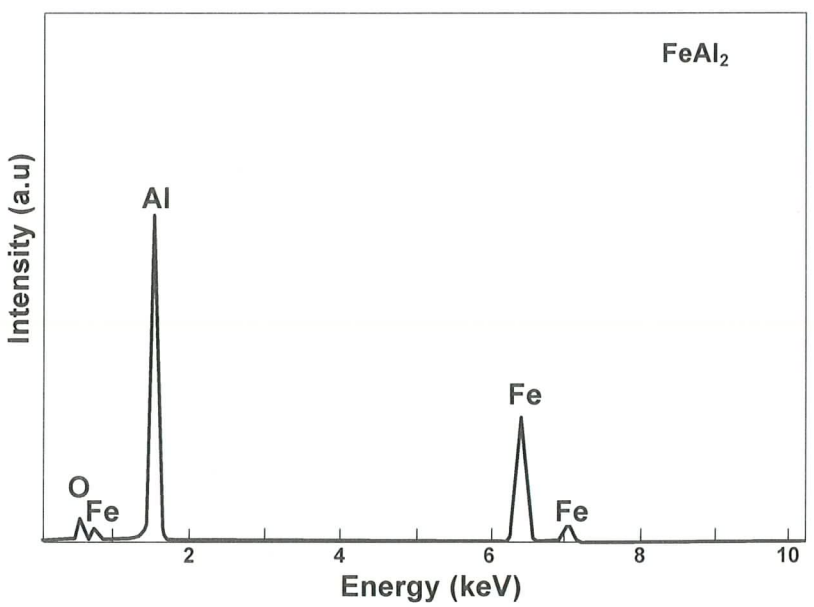

b)

Figure 4.10 a. SEM micrograph of the 3 μm thick aluminum film grown on steel substrate annealed for ½ h at 500^0C, **b.** EDS spectrum of the same film showing the the presence of $FeAl_2$.

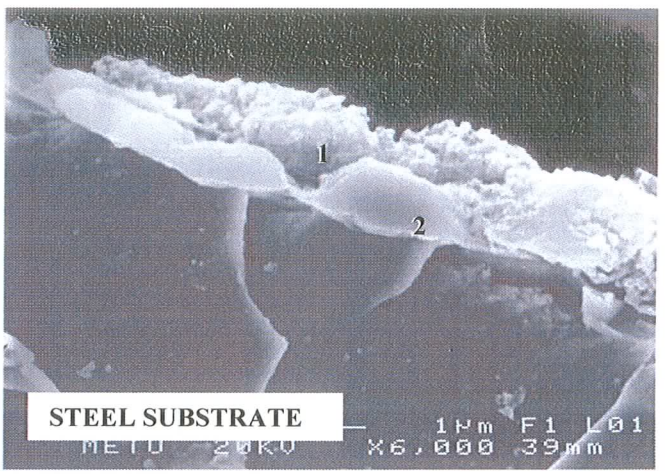

a)

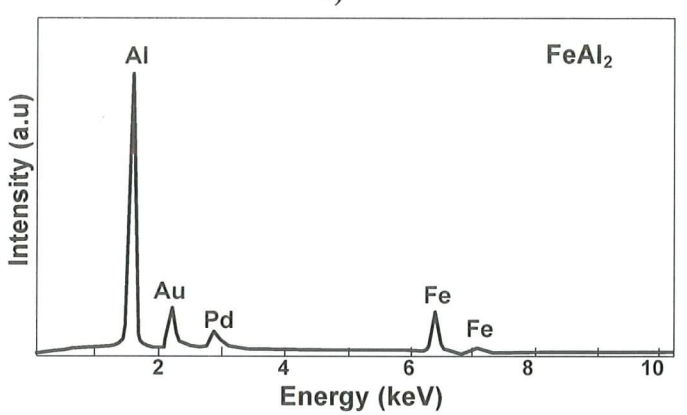

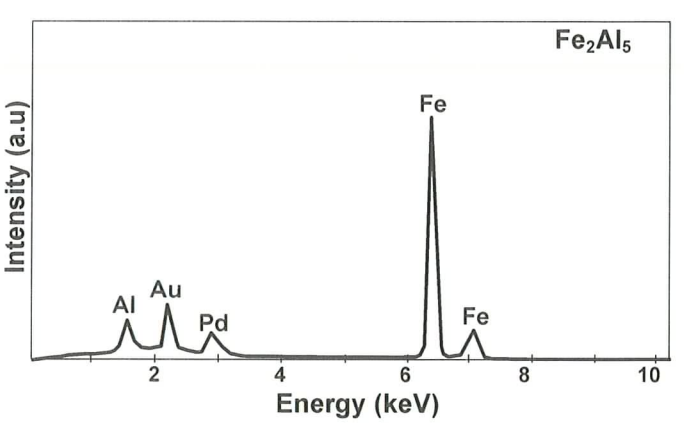

b)

Figure 4.11 a. SEM micrograph of the 8 μm thick aluminum film grown on steel substrate annealed for 3 h at 500^0C, **b.** EDS spectrums of the phases at point "1" and point "2" showing the presence of $FeAl_2$ and Fe_2Al_5 respectively.

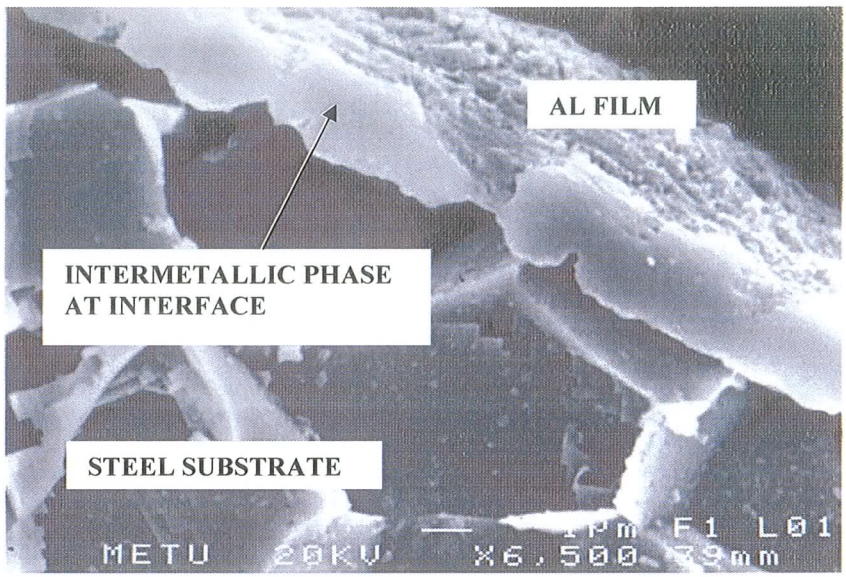

a)

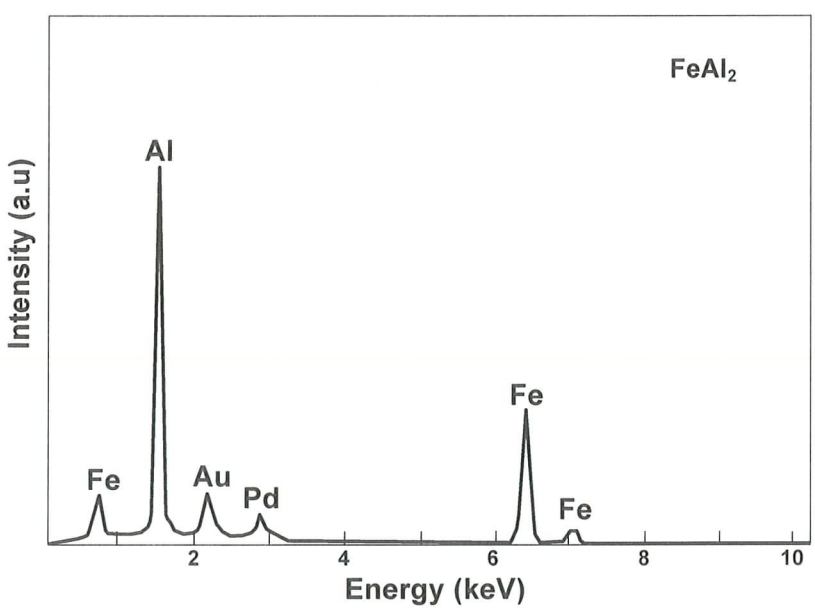

b)

Figure 4.12 a. SEM micrograph of the 14 μm thick aluminum film grown on steel substrate annealed for 3 h at 500^0C, **b.** EDS spectrum of the same film showing the presence of $FeAl_2$.

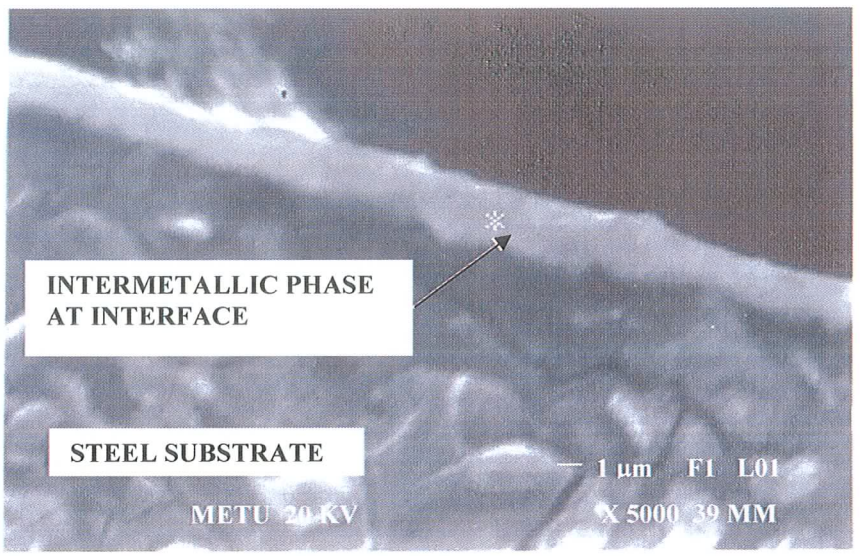

a)

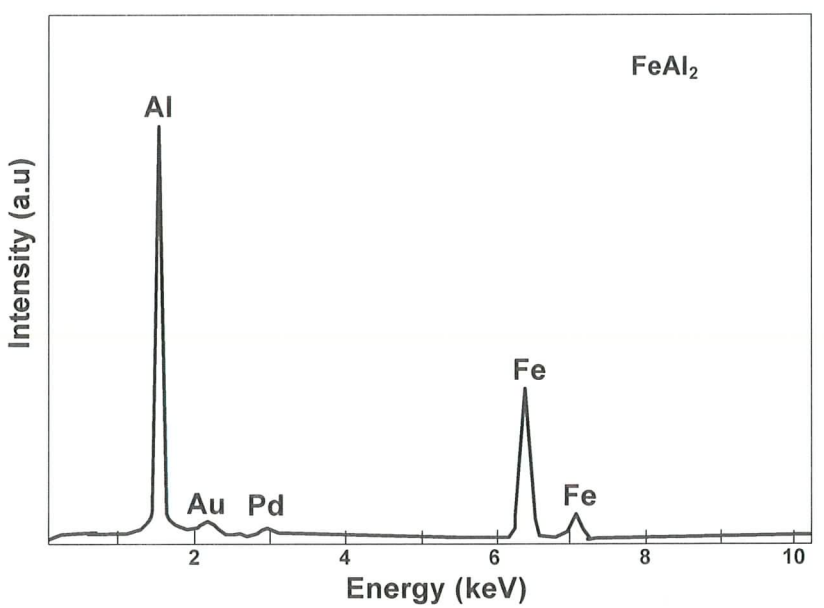

b)

Figure 4.13 a. SEM micrograph of the 14 µm thick aluminum film grown on steel substrate annealed for 8 h at 500^0C, **b.** EDS spectrum of the point "*"showing the presence of $FeAl_2$.

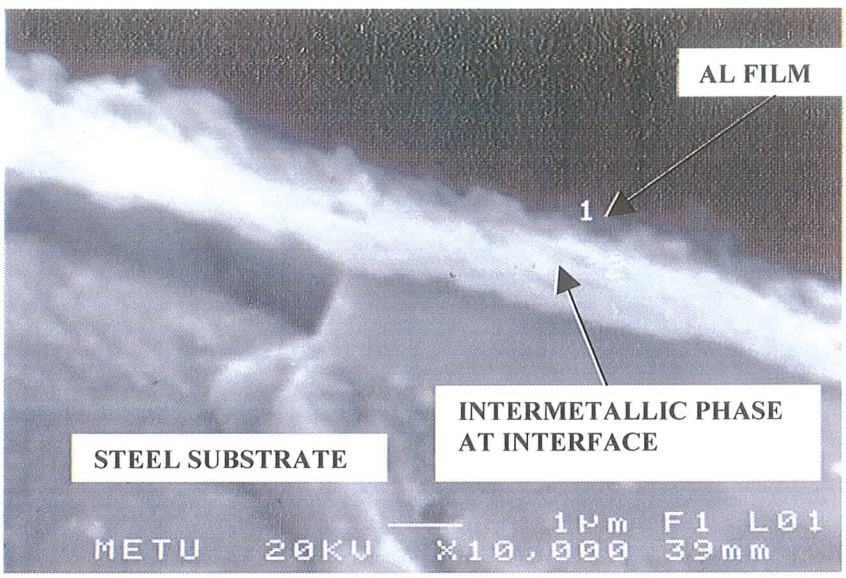

a)

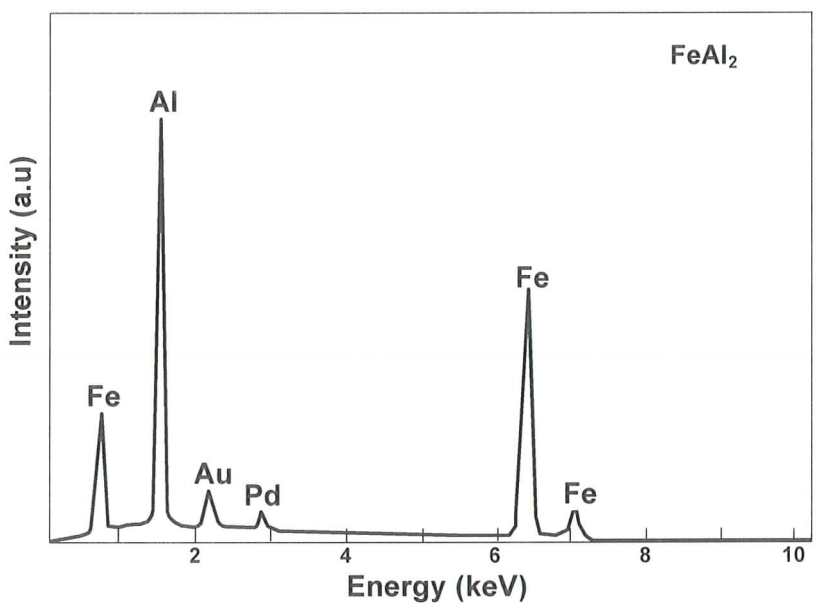

b)

Figure 4.14 a. SEM micrograph of the 8 μm thick aluminum film grown on steel substrate annealed for 4 h at 550^0C, **b.** EDS spectrum of the same film showing the presence of $FeAl_2$.

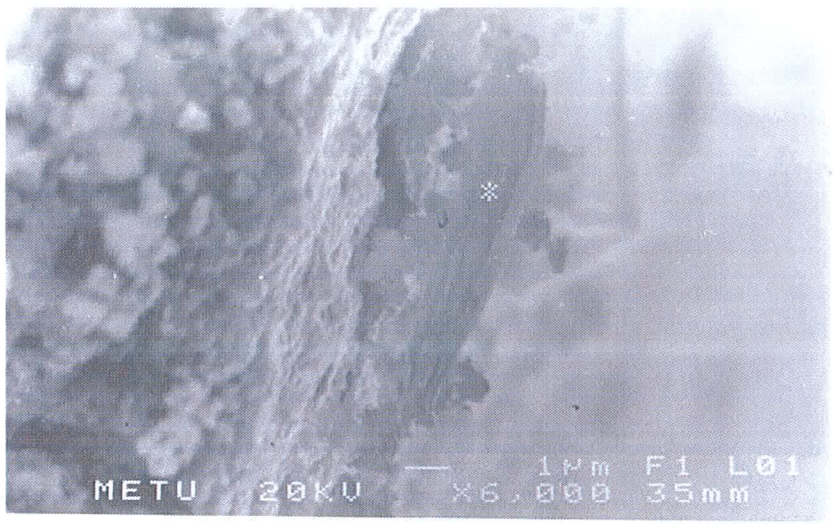

a)

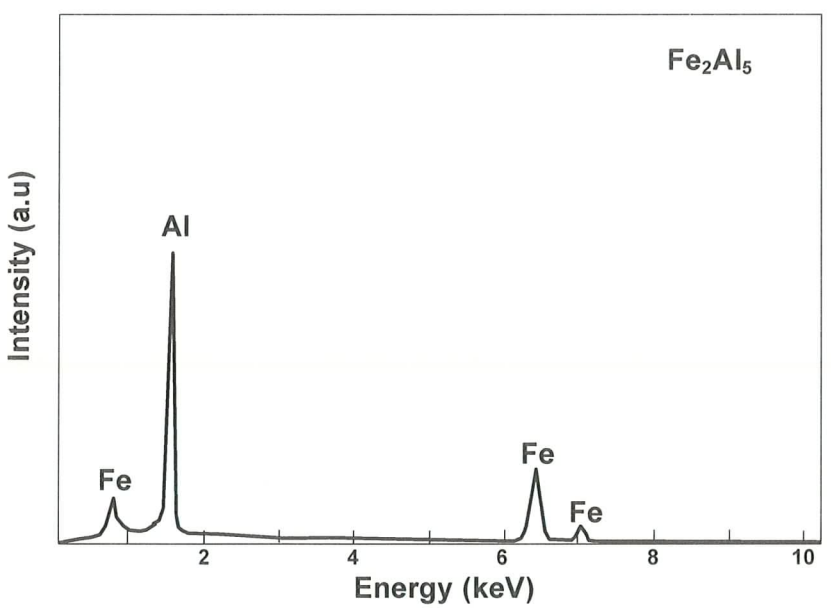

b)

Figure 4.15 a. SEM micrograph of the 3 μm thick aluminum film grown on steel substrate annealed for ½ h at 650^0C, **b.** EDS spectrum of the same film at point "*" showing the presence of Fe_2Al_5.

CHAPTER 5

CONCLUSIONS

Some of the main results can be stated as follows;

The results showed that intermetallic phases $FeAl_2$ and Fe_2Al_5 are the most dominant phases which can be observed and they are formed sequentially on the contrary of intermetallics which formed synchronous in bulk materials.

Intermetallic phase $FeAl_2$ appears first at the Fe - Al film interface at most of the designed experimental conditions. This result is supported thermodynamically as it has lowest free energy of formation in Fe-Al system when compared to other intermetallics at aluminum rich region of the Fe-Al phase diagram.

Intermetallic phase Fe_2Al_5 phase is observed together with intermetallic phase $FeAl_2$ or after the formation of intermetallic phase $FeAl_2$.Three conditions can be set for the formation of intermetallic phase Fe_2Al_5. It is achieved first with increase in annealing time at constant temperature. For moderate initial film thicknesses of 3 μm and 8 μm and at most common annealing temperature of 500^0C sequential formation of intermetallic phase Fe_2Al_5 after intermetallic phase $FeAl_2$ is clearly validated by the experimental results. Secondly it is achieved by decrease of initial film thickness at constant annealing temperature and annealing time. The experimental evidence at 500^0C showed that at constant annealing times of ½ h, and 1 h, formation of intermetallic phase Fe_2Al_5 is seen at lower initial thicknesses; i.e. at 2 μm and not at 3 μm and at 8 μm. The last condition for the formation of intermetallic phase Fe_2Al_5 is to increase annealing

temperature at constant initial aluminum film thickness and at constant annealing time.

Atomic aluminum percentage of the intermetallic phase formed increases with initial aluminum film thickness which is evidenced all through the experiments.

It could also be concluded that with an initial film thickness of 14 μm intermetallic phase $FeAl_2$ is stable for a long period of annealing time at 500^0C. It is expected to be the stable for lower temperatures as well owing same initial film thickness value.

More generally it can be concluded that;

All the phases present in the equilibrium diagram do not necessarily appear and they do not necessarily begin to grow simultaneously but various incubation periods are observed.

Relatively thin initial film thickness and high annealing temperatures favored the formation of more than one compound at once.

The parabolic growth rate of one compound is not the general regime. A compound can not appear because of a nucleation problem (small driving force) or because of a critical thickness required for the neighbor compound. In thin films exhaustion of one constitutive species can be the controlling factor, if it happens before the critical thickness is reached.

REFERENCES

[1] http ://www.met.kth.se.mattechnol / FUMA2002 / IntermetallicApplic/ intermetallics. doc (2006).

[2] R. L. Fleischer, J. of Materials Science 22, 2281 (1987).

[3] N.S. Stoloff, C.T. Liu, S.C. Deevi, Intermetallics 8 1313 (2000).

[4] C. T. Liu, Int. Met. Rev. 29, 168 (1981).

[5] J. J. Petrovic and A. K. Vasudevan, Materials Science and Engineering A 261, 1 (1999).

[6] Wang, Z., Zhou, Y. and Xia, Y., J.Materials Sci., 32, 2387, (1997).

[7] M. Carbucicchio, C. Grazzi ,M. Rateo, G. Ruggiero and G. Turilli NanoStructured Materials, Vol. 11, No. 6, pp. 775-782, (1999).

[8] Özenbaş, M., Güler, H., "Formation of Al-Si Intermetallic Phases", Chem. Eng. Comm. 190: 911-924, (2003).

[9] Hüsniye Güler, "Formation of Intermetallic Phases at the Metal-Silicon Interfaces ", Ph. D. Thesis, Supervisor Prof. Dr. Macit Özenbaş, January 2001, METU, Ankara

[10] J. Philibert, Defect and Diffusion Forum 66-69, 995 (1989).

[11] R. Roy, in Proceedings of the Conference on Phase Transitions and Their Applications in Materials Science, edited by L. E. Cross, pp. 13-27, Pergamon Press, New York, USA, May 23-25, (1973).

[12] V.I.Dybkov, Journal of Materials Science 21, 3085 (1986).

[13] P. Mengucci, G. Majni, A. Di Cristoforo, R. Checchetto, A. Miotello, C. Tosello, G. Principia, Thin Solid Films 433, 205-210, (2003).

[14] Metals Handbook, Vol 63, 10th Edition, ASM International (1992)

[15] M.Potesser, T.Shoeberl, H.Antrekowitsch, J.Bruckner, EPD Congress 167-176, (2006).

[16] S. Makhlouf, M. Shiga, K. Sumiyama: J. Phys. Soc. Jpn. 60, 3537 (1991).

[17] J. Noetzel, D.C. Meyer, A. Tselev, A. Mucklich, P. Paufler, F. Prokert, E. Wieser, W. Moller Appl. Phys. A 71, 47-54 (2000).

[18] Chan-Yeup Chung, Yong-Chae Chung, Materials Letters 60 1063-1067 (2006).

[19] S.-P. Kim, Y.-C. Chung, S.-C. Lee, K.-R. Lee, J. Korean Phys. Soc. 44,18 (2004).

[20] Vikas Jindal, V.C. Srivastava, Arpan Das, R.N. Ghosh, Materials Letters 60, 1758-1761, (2006).

[21] T.B. Massalski (Ed.), Binary Alloy Phase Diagrams, ASM, Metals Park, Ohio, p. 147, (1990).

[22] R. Pretorius, A.M. Vredenberg, F.W. Saris, Journal of Applied Physics 70, 3636,(1971).

[23] I. Ansara, T. Dinsdale, M.H. Rand (Eds.), Thermochemical Database for Light Metal Alloys, vol. 2, COST, Luxembourg, pp. 23-39, (1998).

[24] T. Geilman, J. Chevallier, M. Fanciulli, G. Weyer, V. Nevolin,Zenkevitch, Appl. Surf. Sci. 109-110 570 (1997).

[25] P. Bhattacharya, K.N. Ishihara, K. Chattopadhyay Mater. Sci.Eng. A 304-306 250 (2001).

[26] D.C. Meyer, K. Richter, P. Paufler, P. Gawlitza, T. Holz, J.Appl. Phys. 87 7218 (2000).

[27] A.A. Levin, D.C. Meyer, P. Paufler, A. Gorbunov, A. Tselev, P. Gawlitza, Journal of Alloys and Compounds 320, 114-125, (2001).

[28] Koji Murakami, Norihide Nishida, Kozo Osamura , Yo Tomota, Acta Materialia 52, 1271-1281, (2004).

[29] V. Fleury and L. Balazs, Physica A 233, 640 (1996).

APPENDIX A

CRYSTAL SYSTEMS

Table A.1 Relationships of edge legths and of interaxial angles for the seven crystal systems [14].

Crystal System	Edge Lengths	Interaxial Angles
Triclinic	$a \neq b \neq c$	$\alpha \neq \beta \neq \gamma \neq 90^o$
Monoclinic	$a \neq b \neq c$	$\alpha = \gamma = 90^o \neq \beta$
Orthorhombic	$a \neq b \neq c$	$\alpha = \beta = \gamma = 90^o$
Tetragonal	$a = b \neq c$	$\alpha = \beta = \gamma = 90^o$
Hexagonal	$a = b \neq c$	$\alpha = \beta = 90^o$; $\gamma = 120^o$
Rhombohedral	$a = b = c$	$\alpha = \beta = \gamma \neq 90^o$
Cubic	$a = b = c$	$\alpha = \beta = \gamma = 90^o$

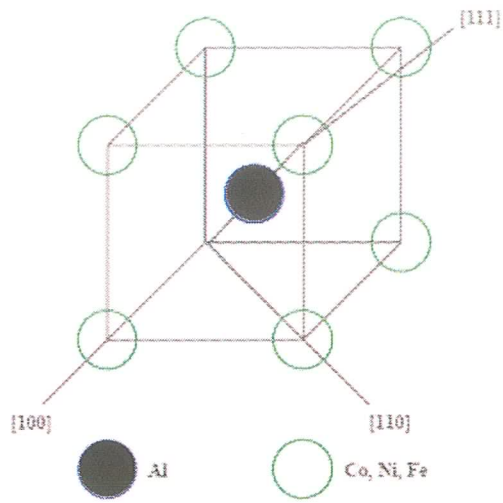

FeAl

a)

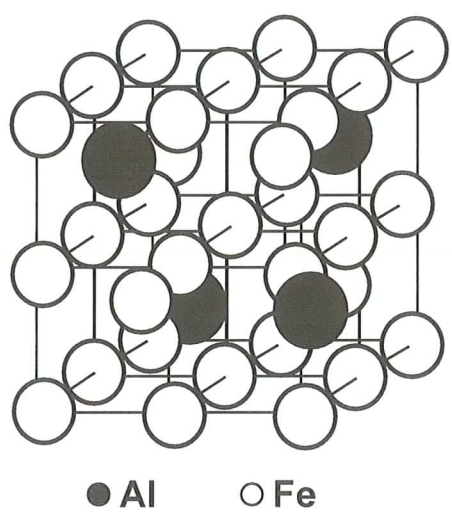

Fe_3Al

b)

Figure A.1 Hard sphere models of crystal structures Fe-Al system a)FeAl (B2) and b) Fe_3Al (D03) [14].

APPENDIX B

XRD SPECTRA OF Al FILMS OF AN INITIAL THICKNESS OF 3 μm GROWN ON STEEL SUBSTRATE ANNEALED FOR DIFFERENT CYCLES AT 500 ^{0}C

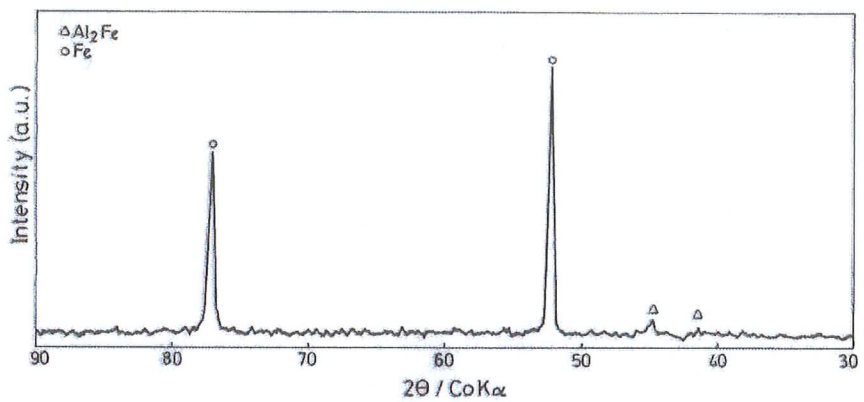

Fig B.1 X-ray diffractogram of Al film of an initial thickness of 8 μm grown on steel substrate annealed for ½ h, at 500 ^{0}C showing the presence of $FeAl_2$.

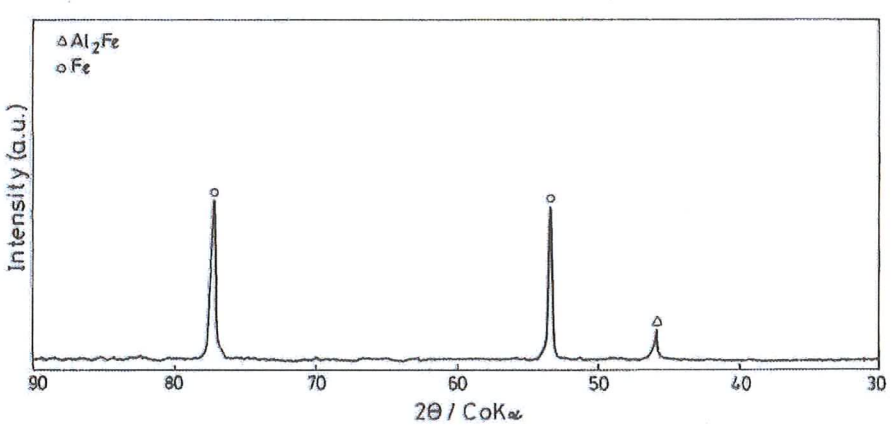

Fig B.2 X-ray diffractogram of Al film of an initial thickness of 8 μm grown on steel substrate annealed for 1 h, at 500 ^{0}C showing the presence of $FeAl_2$.

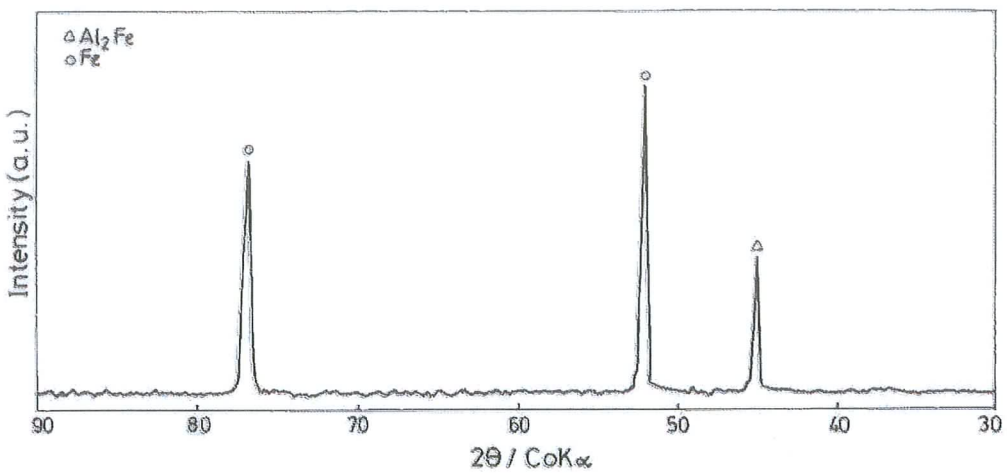

Fig B.3 X-ray diffractogram of Al film of an initial thickness of 8 μm grown on steel substrate annealed for 2 h, at 500 ^{0}C showing the presence of $FeAl_2$.

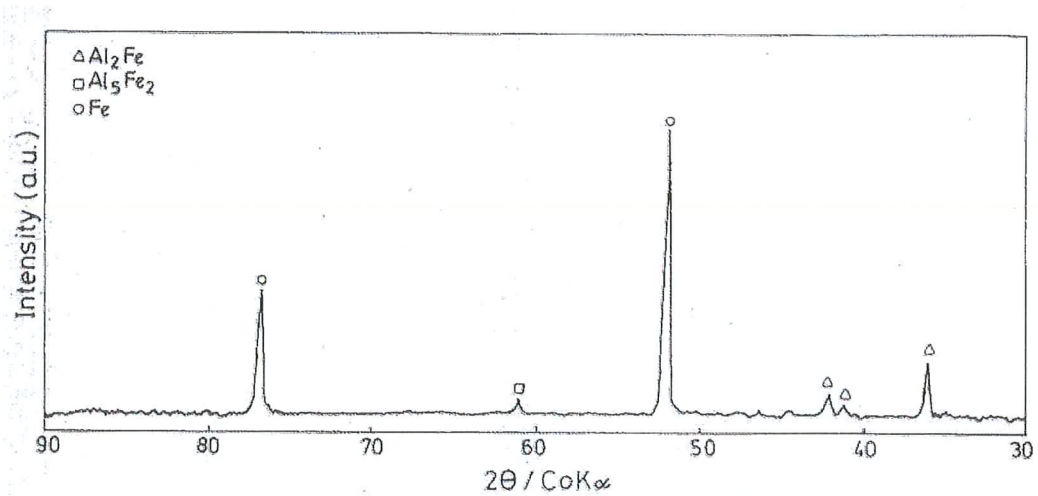

Fig B.4 X-ray diffractogram of Al film of an initial thickness of 8 μm grown on steel substrate annealed for 3 h, at 500 ^{0}C showing the presence of $FeAl_2$ and Fe_2Al_5.

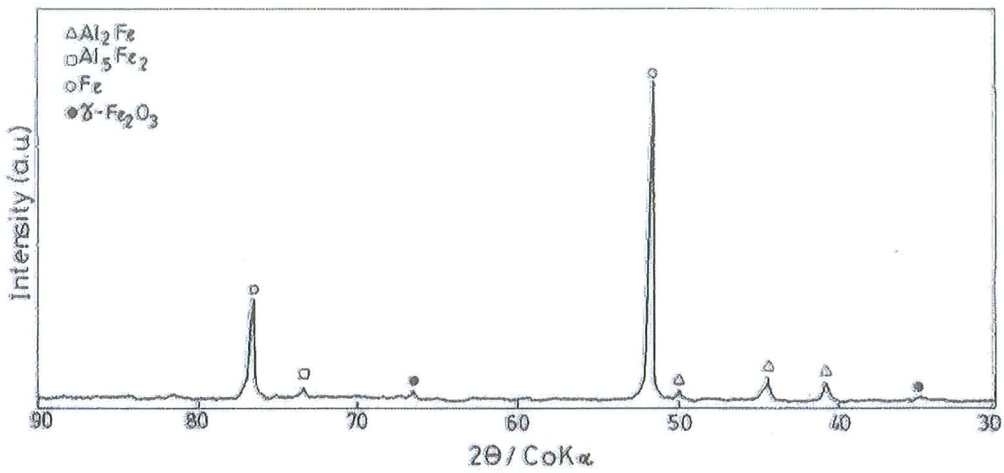

Fig B.5 X-ray diffractogram of Al film of an initial thickness of 8 μm grown on steel substrate annealed for 4 h, at 500 ^{0}C showing the presence of $FeAl_2$ and Fe_2Al_5.

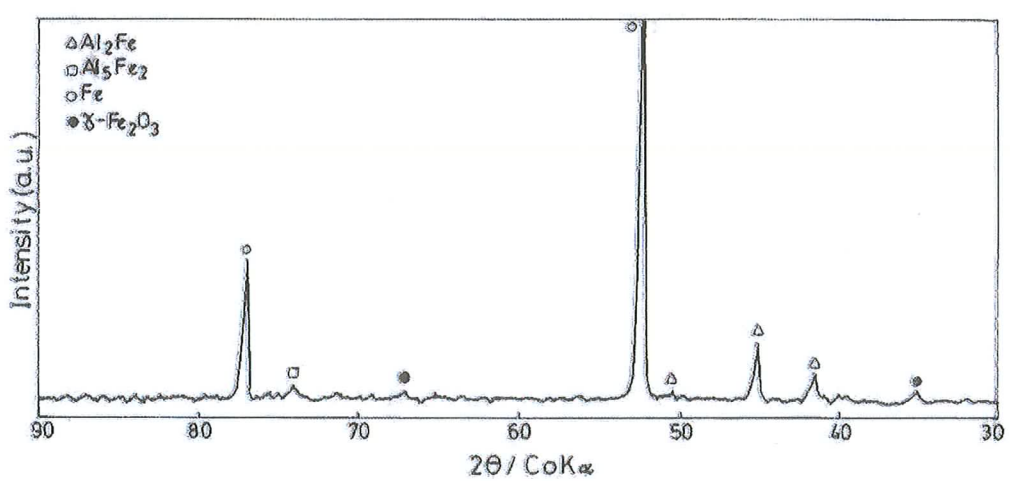

Fig B.6 X-ray diffractogram of Al film of an initial thickness of 8 μm grown on steel substrate annealed for 5 h, at 500 ^{0}C showing the presence of $FeAl_2$ and Fe_2Al_5.

APPENDIX C

XRD SPECTRA OF Al FILMS OF AN INITIAL THICKNESS OF 8 μm GROWN ON STEEL SUBSTRATE ANNEALED FOR DIFFERENT CYCLES AT 500 ^{0}C

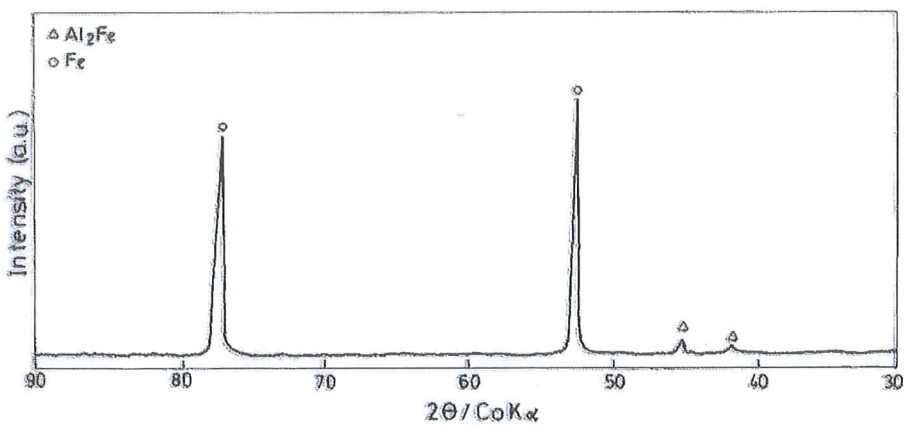

Fig C.1 X-ray diffractogram of Al film of an initial thickness of 3 μm grown on steel substrate annealed for ½ h, at 500 ^{0}C showing the presence of $FeAl_2$.

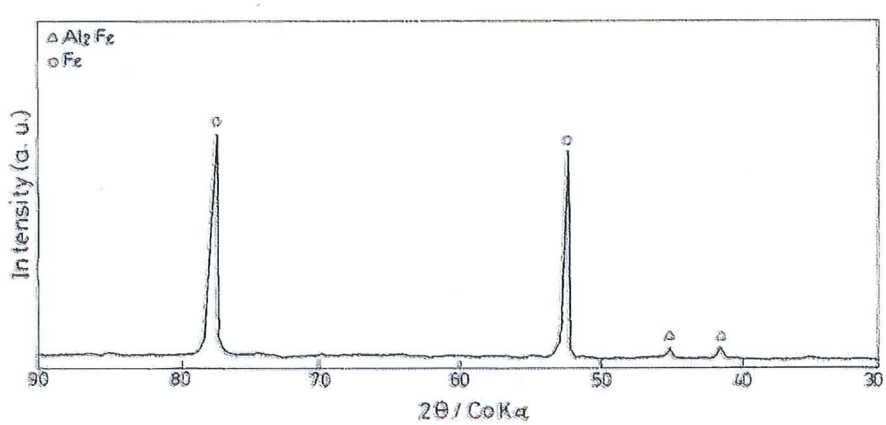

Fig C.2 X-ray diffractogram of Al film of an initial thickness of 3 μm grown on steel substrate annealed for 1 h, at 500 ^{0}C showing the presence of $FeAl_2$.

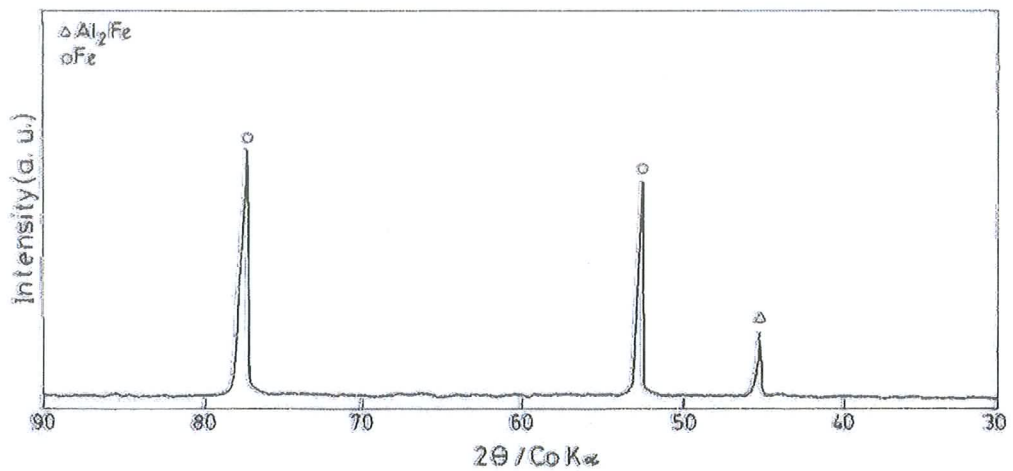

Fig C.3 X-ray diffractogram of Al film of an initial thickness of 3 μm grown on steel substrate annealed for 2 h, at 500 ^{0}C showing the presence of $FeAl_2$.

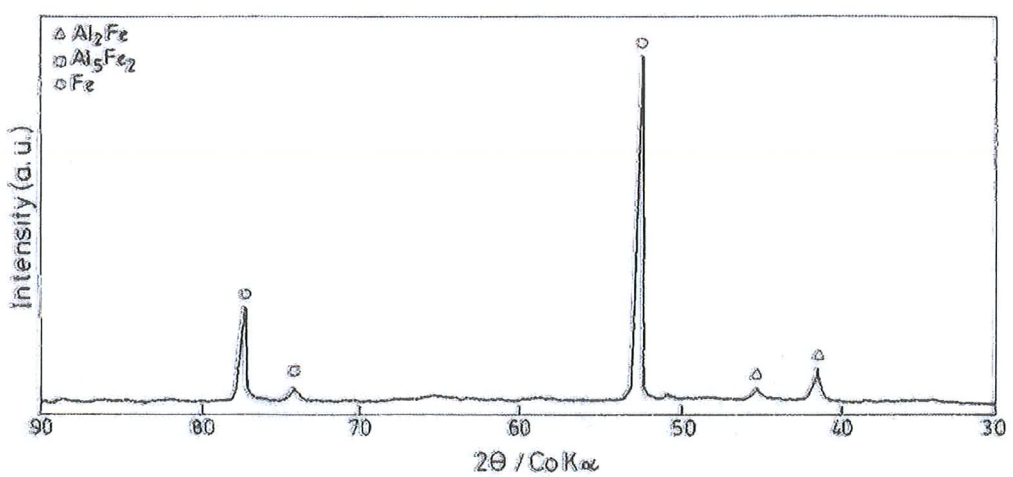

Fig C.4 X-ray diffractogram of Al film of an initial thickness of 3 μm grown on steel substrate annealed for 3 h, at 500 ^{0}C showing the presence of $FeAl_2$ and Fe_2Al_5.

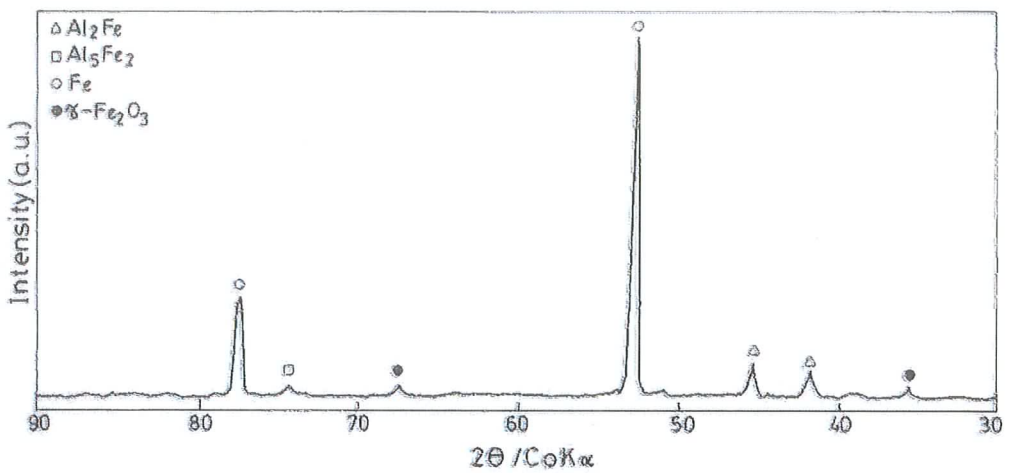

Fig C.5 X-ray diffractogram of Al film of an initial thickness of 3 μm grown on steel substrate annealed for 4 h, at 500 ^{0}C showing the presence of $FeAl_2$ and Fe_2Al_5.

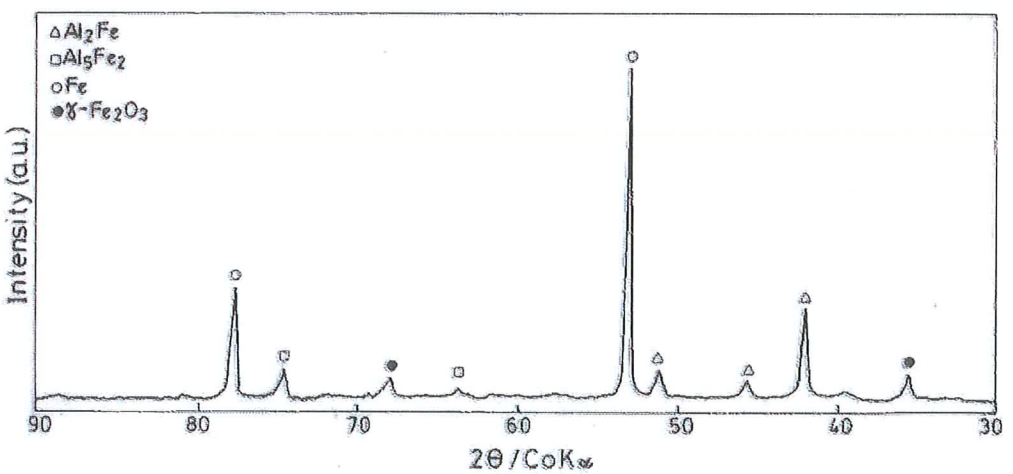

Fig C.6 X-ray diffractogram of Al film of an initial thickness of 3 μm grown on steel substrate annealed for 5 h, at 500 ^{0}C showing the presence of $FeAl_2$ and Fe_2Al_5.